Cooperative Hybrid Beamforming for the Mitigation of Realistic Asynchronous Interference in Cell-free mmWave MIMO Networks

Meesam Jafri, *Student Member, IEEE,* Suraj Srivastava, *Member, IEEE,* Pankaj Kumar, Aditya K. Jagannatham, *Senior Member, IEEE,* and Lajos Hanzo, *Life Fellow, IEEE*

***Abstract*—Cooperative hybrid transmit precoder (TP) and receive combiner (RC) design algorithms are conceived for cell-free millimeter wave (mmWave) multiple-input multiple-output (MIMO) networks, operating in the face of asynchronous interference (ASI). To begin with, a Wiener filtering-based optimal hybrid TP/RC (WHB-U) design is proposed for unicast scenarios that minimizes the normalized mean squared error (NMSE) between the received signal and the desired signal subject to user-specific power constraints. Next, a signal-to-leakage plus noise ratio (SLNR) maximization-based hybrid TP/RC design (SHB-U) is conceived, which reduces the interference engendered by the signal transmission targeted towards a specific user, rather than focuses on the interference at a particular user. Next, a multicast transmission scenario is considered, wherein the users belonging to a particular multicast group request identical information. Toward this, the WHB-M and SHB-M hybrid TP/RC schemes are designed for mitigating both the inter-user and inter-group interference. Subsequently, we also develop a Bayesian learning (BL)-based framework for jointly designing the RF and baseband (BB) TPs/RCs for both unicast and multicast scenarios, which does not require the full knowledge of mmWave MIMO channel components. Finally, the efficiency of the proposed TP/RC schemes is extensively evaluated by simulations both in terms of their ability to mitigate the ASI, and the spectral efficiency attained.**

***Index Terms*—mmWave MIMO, hybrid beamforming, cell-free, multicast, Bayesian learning.**

I. Introduction

Millimeter wave (mmWave) technology has the potential to enable ultra-high bit rates, reduced latencies and large-scale access, due to its ability to leverage the ample bandwidth available in the frequency range spanning 30-300 GHz [1]–[3]. Moreover, the abundant frequency spectrum within the mmWave band has the capacity to support extensive interconnection of devices required by the Internet of Things (IoT) [4]. However, the severe path-loss pose significant challenges for mmWave communication, before its transition from pure research to practical deployment. The philosophy of dense mmWave networks having small cell sizes and distributed base stations (BSs) has shown considerable promise toward overcoming these challenges [5], [6].

However, the network densification results in significant inter-cell interference (ICI), and frequent handovers. To overcome these limitations, the cell-free multiple-input multiple-output (MIMO) paradigm has recently been proposed as a potential architecture for beyond 5G (B5G)/6G wireless networks [7]–[9] and has emerged as a promising solution for enhancing the system throughput attained by surpassing the limitations imposed by the conventional fixed cell architecture. By utilizing multiple cooperative access points (APs) to serve a specific user, a cell-free network enhances the number of spatial degrees of freedom, hence resulting in efficient cooperative transmission and reception [10], [11].

The short wavelength of mmWave signals makes it possible to leverage the benefits of MIMO by placing a large antenna array on devices having compact form factors. Such a MIMO architecture can provide a beamforming gain that is crucial for mmWave systems to mitigate the blockages, atmospheric absorption and penetration losses that are endemic to communication in this band [12]–[14]. However, in a fully digital (FD) signal processing architecture-based conventional MIMO system, each antenna element requires a dedicated RF chain (RFC). The large number of RFCs, arising due to the massive scale of antenna arrays, in turn, leads to significantly higher costs and power consumption, which prohibits the use of FD signal processing in mmWave MIMO systems [1], [15]. A promising solution to overcome this challenge is to exploit the novel hybrid RF baseband (BB) MIMO architecture that utilizes a significantly reduced number of RFCs in comparison to the number of antennas. In such a cooperative cell-free mmWave MIMO network, the interference is inherently asynchronous in nature due to the different propagation delays of the signals arriving from the APs to the users [16]–[18]. Note that perfect timing advance procedures only guarantee the synchronized arrival

The work of Aditya K. Jagannatham was supported in part by the Qualcomm Innovation Fellowship; in part by the Qualcomm 6G UR Gift; and in part by the Arun Kumar Chair Professorship.

L. Hanzo would like to acknowledge the financial support of the Engineering and Physical Sciences Research Council projects EP/W016605/1, EP/X01228X/1, EP/Y026721/1 and EP/W032635/1 as well as of the European Research Council's Advanced Fellow Grant QuantCom (Grant No. 789028)

M. Jafri, P. Kumar, and A. K. Jagannatham are with the Department of Electrical Engineering, Indian Institute of Technology Kanpur, Kanpur, 208016, India (e-mail: meesam@iitk.ac.in, kpankaj21@iitk.ac.in, adityaj@iitk.ac.in.). S. Srivastava is with the Department of Electrical Engineering, Indian Institute of Technology Jodhpur, Jodhpur, 342030, India (e-mail: surajsri@iitj.ac.in). L. Hanzo is with the School of Electronics and Computer Science, University of Southampton, Southampton SO17 1BJ, U.K. (e-mail: lh@ecs.soton.ac.uk)

of signals from different APs at their intended receivers. Thus, designing the RF and BB transmit precoders (TPs) and receive combiners (RCs) in the presence of asynchronous interference (ASI) plays a pivotal role in harnessing the substantial benefits offered by cooperative cell-free mmWave MIMO communication for 5G/B5G networks. A brief review of the existing contributions in this context is presented next.

A. State-of-the-art

In recent years, sophisticated beamformer design techniques have been proposed for mmWave multi-cell multi-user MIMO systems [19]–[22]. Michaloliakos *et al.* [19] proposed a novel analog TP design which maximizes the capacity by exploiting a set of predefined beam patterns. Zhang *et al.*, in their path-breaking work [20], conceived signal-to-interference leakage-plus-noise ratio (SLNR) maximization-based distributed linear TP designs for cooperative multi-cell systems that rely on reduced information exchange amongst the BSs. Xiang *et al.* [21] proposed a coordinated beamformer scheme, which maximizes the signal-to-interference noise ratio (SINR), while incorporating realistic per BS power constraints. The authors of [22] proposed coordinated TP design for multi-cell networks based on the maximization of the weighted sum energy efficiency.

There are however only very few contributions that explore the cooperative TP design of cell-free MIMO networks. Early works in this area designed the FD beamformer for conventional cell-free MIMO systems [11], [23]–[25]. Nayebi *et al.* [23] proposed a centralized zero-forcing (ZF) TP design which significantly improves the achievable data rates of cell-free MIMO networks. Masoud *et al.* [24] proposed a modified conjugate beamformer technique for cell-free systems that completely avoids self-interference, with no action required at the receivers. The proposed scheme remarkably improves the achievable downlink data rates in comparison to conjugate beamforming. Björnson *et al.* [11] studied the various levels of cooperation between the APs and developed minimum mean square error (MMSE)-based TP algorithms for improving the overall spectral efficiency. The implementation architectures proposed for cell-free systems lead to a significant reduction in backhaul signalling overheads. Furthermore, the authors of [25] derived MMSE-based cooperative centralized TPs by exploiting the downlink-uplink duality. Cao *et al.* [26] proposed a specific reference signal for an over-the-air reciprocity calibration scheme to avoid channel state information (CSI) feedback in time-division duplex for cell-free massive MIMO systems.

Some authors have also explored the hybrid TPs designed for cell-free mmWave MIMO networks. Hou *et al.* [27] proposed a two-stage framework for the design of the hybrid TP in cooperative cell-free networks. In the first stage, the RF TP is obtained from a predefined codebook, while the BB TP is obtained in the second stage by employing the popular semidefinite relaxation (SDR) algorithm. Kim *et al.* [28] proposed a weighted MMSE (WMMSE) criterion based hybrid TP design, where the RF and BB TPs are computed via the alternate optimization framework. The authors of [29] maximized the weighted sum rate (WSR) of all the users in the network by employing a block coordinate descent (BCD) algorithm for deriving the hybrid TPs. Authors in [30] proposed a WSR maximization and max-min fairness based two-stage hybrid beamformer design. In the first stage, analog beamformers are designed for APs during uplink training. Subsequently, the baseband beamformer is obtained by employing the effective baseband channel in the second stage. He *et al.* [31] proposed an energy-efficient hybrid beamformer design based on an iterative heuristic Gram-Schmidt algorithm for cell-free wideband mmWave MIMO systems. In [32], the authors considered a reflective intelligent surface (RIS)-aided cell-free mmWave MIMO system and designed the cooperative beamformer by maximizing the WSR. In [33], the authors proposed a hybrid TPC scheme for cell-free mmWave MIMO networks that maximizes the user rate. In [34], the authors conceived a minimum variance distortionless response (MVDR)-based hybrid TP framework for cooperative cell-free mmWave MIMO networks for mitigating the multi-user interference (MUI).

Note however that all the above papers consider synchronous interference, which is based on the assumption that each user is able to receive both the desired and the interfering signals transmitted by all the APs synchronously. However, it must be emphasized that the interference in a cell-free network is fundamentally asynchronous in nature. Due to the inevitable difference in propagation delays of the signals between the APs and several users, it is not possible for the APs to align all the interfering signals at all the users, which leads to ASI. Ignoring this property can significantly degrade the efficiency of the cooperative beamformer design of cell-free networks. In this context, the authors of [35] derived the MMSE-based channel estimator considering the ASI in cell-free MIMO systems, wherein each user is equipped with a single receive antenna. Li *et al.* [36] proposed MMSE-based channel estimation and maximum ratio combining (MRC)-based TP schemes under asynchronous signal reception in a cell-free MIMO-aided orthogonal frequency division multiplexing (OFDM) system. The authors of [37] proposed a rate-splitting based transmission framework to mitigate the problem of asynchronous reception of signals caused by both propagation delays and oscillator phases of the transceivers. Although these contributions studied the effects of ASI in cell-free networks, there is a notable scarcity of contributions addressing the challenges associated with the high-frequency mmWave band, as discussed earlier. To the best of our knowledge, the problem of ASI in cell-free mmWave MIMO networks has not been tackled in the existing literature. Therefore, to address this knowledge gap in the existing research literature, this paper proposes a cooperative asynchronous hybrid TP/RC design for a cell-free multi-user mmWave MIMO network. The contributions of this paper are boldly and explicitly contrasted to the literature in Table I. It can be readily observed from I that

the contributions of this work are significant, since none of the existing papers in the literature comprehensively develop beamformers for mitigating the degrading effects of ASI in cell-free mmWave MIMO networks. The key novelty of our current study is to develop a hybrid beamformer considering different performance metrics for the mitigation of ASI. Our key contributions are detailed below.

B. Contributions

This treatise proposed efficient hybrid TP/RC techniques for cell-free mmWave MIMO networks with ASI for both unicast and multicast scenarios.

- To begin with, a model is developed for cooperative hybrid beamforming to mitigate the ASI in cell-free mmWave MIMO networks. The Wiener hybrid beamforming (WHB) principle is then employed for the design of the hybrid TP/RC that minimizes the overall normalized mean squared error (NMSE) subject to user-specific power constraints, considering the availability of angles of arrival/departure (AoAs/AoDs) and path gains of the multipath components in a unicast scenario.
- Next, an SLNR-based hybrid beamforming (SHB) scheme is proposed for the unicast scenario to determine the TP/RC weights, which maximize the SLNR of each user. This framework differs from all the previous ones in that it aims for reducing the interference originating due to the signal transmission targeted towards a specific user, rather than focus on the interference at a particular user. Note that NMSE and SLNR are employed as popular metrics to solve the hybrid beamformer design problems in [38]–[41]. However, these studies do not incorporate the ASI and are limited to a single data stream per user.
- Next, the design and analysis of the proposed schemes are extended to multicast transmission scenarios, wherein the users belonging to a particular multicast group request identical information. Toward this, the NMSE and SLNR-based hybrid TP/RC schemes are designed for mitigating both the MUI and inter-group interference.
- Subsequently, a Bayesian learning (BL)-based framework is introduced for the design of the RF and BB constituents of the hybrid TP, which is highly valuable in scenarios, where precise information about the AoAs/AoDs and the associated path gains of mmWave channel is not available.
- Finally, simulation results are presented to demonstrate the efficacy of the proposed WHB and SHB schemes in mitigating the ASI in addition to the enhanced spectral efficiency in comparison to conventional ZF interference nulling. It is also shown that the performance attained by the proposed algorithms approaches that of the ideal FD transceiver.

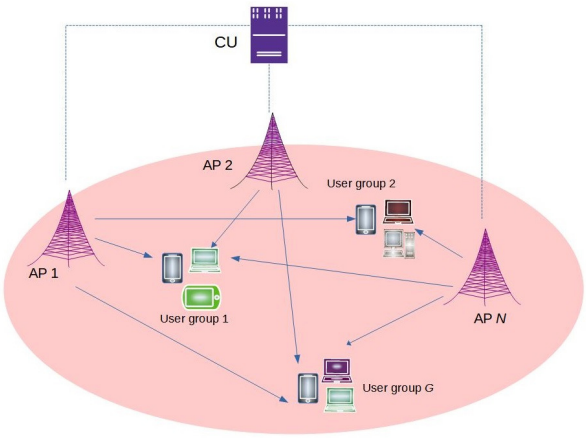

Fig. 1: System model for a cooperative cell-free mmWave MIMO network

C. Notations

Vectors and matrices are denoted by boldfaced lower and uppercase letters, respectively, while scalars are represented by lowercase letters. The transpose, Hermitian, conjugate, and inverse of a matrix $\mathbf{F}$ are denoted by $\mathbf{F}^T$, $\mathbf{F}^H$, $\mathbf{F}^*$, and $\mathbf{F}^{(-1)}$ respectively. $\mathrm{Tr}(\mathbf{F})$ denotes the trace of a matrix $\mathbf{F}$, $\|\mathbf{x}\|_2$ represents the l_2 norm of a vector, while $\|\mathbf{A}\|_F$ denotes the Frobenious norm of a matrix $\mathbf{A}$. $\mathbb{E}[.]$ signifies the expectation operator. Furthermore, $\mathbf{x} \sim \mathcal{CN}(\mathbf{b}, \mathbf{A})$ denotes a complex Gaussian random vector with mean $\mathbf{b}$ and covariance matrix $\mathbf{A}$. $\mathbf{I}$ represents an identity matrix.

II. System Model

The cell-free mmWave hybrid MIMO downlink system consists of N cooperative APs, wherein the APs are connected to a control unit (CU) and jointly serve G user groups. We assume that all APs serve all users, similar to the related works [29], [37]. The group g is comprised of U_g users, as illustrated in Fig. 1. The nth AP is equipped with N_T transmit antennas (TAs) and $N_{\mathrm{RF},n}$ RFCs to transmit K streams such that $K \leq N_{\mathrm{RF},n} << N_T$, $\forall\ 1 \leq n \leq N$. Each user is equipped with N_R receive antennas (RAs) and $N_{\mathrm{RF},u}$ RFCs, satisfying $K \leq N_{\mathrm{RF},u} \leq N_R$. We consider a general multicast scenario, where multiple users request the same data and rely on identical services. Let the uth user in the gth group be represented by $U_u^{(g)}$. Since the APs are located in different geographical positions, their transmissions to the users experience different propagation delays. The desired signals intended for a particular user, which are transmitted from all the cooperative APs, reach the user synchronously. This can be achieved via a timing synchronization mechanism. However, the APs cannot perfectly line up all the interfering signals at each user due to the difference in propagation times between the APs and users. Therefore, the interference at user $U_u^{(g)}$ arising from the APs due to the transmission to other users in the system is asynchronous in nature with the desired signal of user $U_u^{(g)}$. This, in turn, depends upon the distance between an

TABLE I: Contrasting contributions to the existing literature

	[15]	[19]	[21]	[22]	[23]	[24]	[25]	[27]	[28]	[29]	[30]	[34]	[36]	[37]	Proposed Work
mmWave communication	✓	✓						✓	✓	✓	✓	✓			✓
Hybrid architecture	✓	✓						✓	✓	✓	✓	✓			✓
Multi-user		✓	✓	✓	✓	✓	✓	✓	✓	✓	✓	✓	✓	✓	✓
Multi-stream	✓	✓		✓						✓					✓
Cooperative beamforming		✓	✓	✓	✓		✓				✓	✓	✓	✓	✓
Multicast multi-group			✓									✓		✓	✓
Unicast		✓	✓	✓	✓	✓	✓	✓	✓	✓	✓	✓	✓	✓	✓
Cell-free					✓	✓	✓	✓	✓	✓	✓	✓	✓	✓	✓
Asynchronous interference													✓	✓	✓
BL-based design															✓

AP and a user. Suffice to say that most standardized wireless systems rely on adaptive time-frame alignment, where the APs appropriately estimate their propagation delays and advance their transmissions, so that they arrive at the user within the required time window. However, this technique fails to mitigate the interference. But again, in this work, we assume that the ASI arises mainly from a difference in the propagation delays, while the case with hardware oscillator errors and imperfect CSI is set aside for future research [35], [36]. Let $\tau_{n,u}^{(g)}$ denote the propagation delay from the nth AP to user $U_u^{(g)}$. The timing advance $\delta_{n,u}^{(g)}$ for the user $U_u^{(g)}$ due to transmission by the nth AP, so that all the signals arrive simultaneously, can be modeled as

$$\delta_n^{(g)} = \tau_n^{(g)} - \tau_{n_g}^{(g)}, \tag{1}$$

where n_g denotes the AP that is closest to the gth user group. The signal $\tilde{\mathbf{r}}_u^{(g)}(t) \in \mathbb{C}^{N_{\mathrm{RF},u}\times 1}$ received at the user $U_u^{(g)}$ after RF combining can be expressed as

$$\begin{aligned}\tilde{\mathbf{r}}_u^{(g)}(t) = \sum_{m=0}^{\infty}\Bigg\{\sum_{n=1}^{N}\left(\mathbf{W}_{\mathrm{RF},u}^{(g)}\right)^H \mathbf{H}_{u,n}^{(g)}\mathbf{F}_{\mathrm{RF},n}\mathbf{F}_{\mathrm{BB},n}^{(g)}\mathbf{x}^{(g)}(m)\\ p\left(t-mT-\tau_{n_{u(g)},u}^{(g)}\right)\Bigg\} + \sum_{m=0}^{\infty}\Bigg\{\sum_{\substack{l=1\\l\neq g}}^{G}\sum_{n=1}^{N}\left(\mathbf{W}_{\mathrm{RF},u}^{(g)}\right)^H\\ \mathbf{H}_{u,n}^{(g)}\mathbf{F}_{\mathrm{RF},n}\mathbf{F}_{\mathrm{BB},n}^{(l)}\mathbf{x}^{(l)}(m)p\left(t-mT-\tau_n^{(g)}+\delta_n^{(l)}\right)\Bigg\}\\ +\left(\mathbf{W}_{\mathrm{RF},u}^{(g)}\right)^H\tilde{\mathbf{v}}_u^{(g)}(t),\end{aligned} \tag{2}$$

where $\mathbf{H}_{u,n}^{(g)} \in \mathbb{C}^{N_R\times N_T}$ and $\mathbf{x}^{(g)}(m)$ denote the mmWave MIMO channel matrix from the nth AP to the user $U_u^{(g)}$ and the signal transmitted by the nth AP to the gth user group, respectively. Furthermore, $\mathbf{F}_{\mathrm{RF},n} \in \mathbb{C}^{N_T\times N_{\mathrm{RF},n}}$ represents the RF TP and $\mathbf{F}_{\mathrm{BB},n}^{(g)} \in \mathbb{C}^{N_{\mathrm{RF},n}\times K}$ denotes the BB TP utilized by the nth AP for its transmission to the gth group. Furthermore, $\mathbf{W}_{\mathrm{RF},u}^{(g)} \in \mathbb{C}^{N_R\times N_{\mathrm{RF},u}}$ denotes the RF combiner employed by the uth user in the gth group, $p(t)$ represents the unit-energy BB signature waveform of duration T and $\tilde{\mathbf{v}}_u^{(g)}(t) \in \mathbb{C}^{N_R\times 1}$ denotes the additive white Gaussian noise (AWGN) vector with distribution $\mathcal{CN}(0,\sigma^2\mathbf{I})$. The received signal $\mathbf{r}_u^{(g)}(t)$ is passed through a filter matched to $p\left(t-mT-\tau_{n^g}^{(g)}\right)$, which is delayed by $\tau_{n^g}^{(g)}$. The signal $\tilde{\mathbf{r}}_u^{(g)}(m)$ received at the output of the matched filter after BB combining can be expressed as

$$\begin{aligned}\mathbf{r}_u^{(g)}(m) = \sum_{n=1}^{N}\left(\mathbf{W}_{\mathrm{RF},u}^{(g)}\mathbf{W}_{\mathrm{BB},u}^{(g)}\right)^H\mathbf{H}_{u,n}^{(g)}\mathbf{F}_{\mathrm{RF},n}\mathbf{F}_{\mathrm{BB},n}^{(g)}\mathbf{x}^{(g)}(m)\\ +\sum_{\substack{l=1\\l\neq g}}^{G}\sum_{n=1}^{N}\left(\mathbf{W}_{\mathrm{RF},u}^{(g)}\mathbf{W}_{\mathrm{BB},u}^{(g)}\right)^H\mathbf{H}_{u,n}^{(g)}\mathbf{F}_{\mathrm{RF},n}\mathbf{F}_{\mathrm{BB},n}^{(l)}\boldsymbol{\nu}_n^{(l,g)}(m)\\ +\mathbf{W}_{\mathrm{BB},u}^{(g)}\mathbf{W}_{\mathrm{RF},u}^{(g)}\tilde{\mathbf{v}}_u^{(g)}(m),\end{aligned} \tag{3}$$

where the quantity $\boldsymbol{\nu}_n^{(l,g)}(m) \in \mathbb{C}^{K\times 1}$ denotes the ASI at the gth user group due to the signal transmitted by the nth AP for the user group l. The ASI is dependent on the difference between the timing-advances $\tau_n^{(l,g)}$ used by AP n for the multicast groups l and g:

$$\tau_n^{(l,g)} = (\tau_n^{(g)} + \delta_n^{(l)}) - \tau_{n_g}^{(g)} = \delta_n^{(g)} - \delta_n^{(l)}. \tag{4}$$

In (3), the ASI term $\boldsymbol{\nu}_n^{(l,g)}(m)$ at group g emerges from two successive symbols, for example, with indices $m_n^{(l,g)}$ and $m_n^{(l,g)}+1$, that are transmitted to group g from AP n. Let $\delta_n^{(l,g)} = \tau_n^{(l,g)} \bmod T$. Then, we have:

$$\begin{aligned}\boldsymbol{\nu}_n^{(l,g)}(m) = \rho(\delta_n^{(l,g)}-T)\mathbf{x}^{(g)}(m_n^{(l,g)})\\ +\rho(\delta_n^{(l,g)})\mathbf{x}^{(g)}(m_n^{(l,g)}+1),\end{aligned} \tag{5}$$

where $\rho(\tau) = \int_0^T g(m)g(t-\tau)dt$ with $\rho(0)=1$. Let us define the effective channel matrix between the nth AP and the user $U_u^{(g)}$ as $\tilde{\mathbf{H}}_{u,n}^{(g)} = \left(\mathbf{W}_{\mathrm{RF},u}^{(g)}\right)^H\mathbf{H}_{u,n}^{(g)}\mathbf{F}_{\mathrm{RF},n} \in \mathbb{C}^{N_{\mathrm{RF},u}\times N_{\mathrm{RF},n}}$. Thus, the system model in (3) can be recast as

$$\begin{aligned}\mathbf{r}_u^{(g)}(m) = \sum_{n=1}^{N}\left(\mathbf{W}_{\mathrm{BB},u}^{(g)}\right)^H\tilde{\mathbf{H}}_{u,n}^{(g)}\mathbf{F}_{\mathrm{BB},n}^{(g)}\mathbf{x}^{(g)}(m)\\ +\sum_{\substack{l=1\\l\neq g}}^{G}\left(\mathbf{W}_{\mathrm{BB},u}^{(g)}\right)^H\sum_{n=1}^{N}\tilde{\mathbf{H}}_{u,n}^{(g)}\mathbf{F}_{\mathrm{BB,n}}^{(l)}\boldsymbol{\nu}_n^{(l,g)}(m)+\mathbf{v}_u^{(g)}(m),\end{aligned} \tag{6}$$

where $\mathbf{v}_u^{(g)}(m) = \left(\mathbf{W}_{\mathrm{BB},u}^{(g)}\right)^H\left(\mathbf{W}_{\mathrm{RF},u}^{(g)}\right)^H\tilde{\mathbf{v}}_u^{(g)}(m)$. Let us also define the concatenated BB TP $\mathbf{F}_{\mathrm{BB}}^{(g)} \in \mathbb{C}^{\tilde{N}\times K}$, where $\tilde{N} = \sum_{n=1}^{N} N_{\mathrm{RF},n}$, for the gth group as $\mathbf{F}_{\mathrm{BB}}^{(g)} = \left[\left(\mathbf{F}_{\mathrm{BB},1}^{(g)}\right)^H, \left(\mathbf{F}_{\mathrm{BB},2}^{(g)}\right)^H, \ldots, \left(\mathbf{F}_{\mathrm{BB},M}^{(g)}\right)^H\right]^H$. The concatenated effective channel matrix between the user $U_u^{(g)}$

and all the cooperating APs is defined as $\tilde{\mathbf{H}}_u^{(g)} = [\tilde{\mathbf{H}}_{u,1}^{(g)}, \tilde{\mathbf{H}}_{u,2}^{(g)}, \ldots, \tilde{\mathbf{H}}_{u,N}^{(g)}] \in \mathbb{C}^{N_{\mathrm{RF},u} \times \tilde{N}}$. Therefore, the effective received signal at user $U_u^{(g)}$ can be written as

$$\mathbf{r}_u^{(g)}(m) = \mathbf{W}_{\mathrm{BB},u}^{(g)} \tilde{\mathbf{H}}_u^{(g)} \mathbf{F}_{\mathrm{BB}}^{(g)} \mathbf{x}^{(g)}(m) + \sum_{\substack{l=1 \\ l \neq g}}^{G} \sum_{n=1}^{N} \mathbf{W}_{\mathrm{BB},u}^{(g)} \tilde{\mathbf{H}}_n^{(g)} \mathbf{F}_{\mathrm{BB,n}}^{(l)} \boldsymbol{\nu}_n^{(l,g)}(m) + \mathbf{v}_u^{(g)}(m). \quad (7)$$

Furthermore, upon considering perfect synchronization, i.e. synchronous interference, the expression in (7) reduces to the following one

$$\mathbf{r}_u^{(g)}(m) = \mathbf{W}_{\mathrm{BB},u}^{(g)} \tilde{\mathbf{H}}_u^{(g)} \mathbf{F}_{\mathrm{BB}}^{(g)} \mathbf{x}^{(g)}(m) + \sum_{\substack{l=1 \\ l \neq g}}^{G} \mathbf{W}_{\mathrm{BB},u}^{(g)} \tilde{\mathbf{H}}_u^{(g)} \mathbf{F}_{\mathrm{BB}}^{(l)} \mathbf{x}^{(l)}(m) + \mathbf{v}_u^{(g)}(m). \quad (8)$$

A. mmWave MIMO channel model

The propagation environment between the APs and users is modeled as a geometric channel comprising L dominant multipath components in the mmWave MIMO system [1], [15]. Under this model, the mmWave channel matrix $\mathbf{H}_{n,u} \in \mathbb{C}^{N_R \times N_T}$ of the link spanning from the nth AP to the uth user can be expressed as

$$\mathbf{H}_{n,u} = \sqrt{\frac{N_R \times N_T}{L}} \sum_{l=1}^{L} \beta_{n,u}^{(l)} \mathbf{a}_R(\phi_{l,n,u}^R) \mathbf{a}_T^H(\phi_{l,n,u}^T), \quad (9)$$

where $\beta_{n,u}^{(l)}$, $\phi_l^R \in [0, 2\pi]$ and $\phi_l^T \in [0, 2\pi]$ denote the complex path gain, AoA and AoD, respectively, associated with the lth multipath component. Let λ and d denote the signal wavelength and antenna spacing, respectively. The quantities $\mathbf{a}_R(\phi_l^R)$ and $\mathbf{a}_T(\phi_l^T)$ represent the receive and transmit array manifold vectors, respectively, corresponding to the lth path, which are defined for a uniformly spaced linear arrays (ULA) as

$$\mathbf{a}_R(\phi_l^R) = \frac{1}{\sqrt{N_R}} [1, e^{j\frac{2\pi}{\lambda} d \sin(\phi_l^R)}, ..., e^{j\frac{2\pi}{\lambda}(N_R-1) d \sin(\phi_l^R)}]^T.$$

$$\mathbf{a}_T(\phi_l^T) = \frac{1}{\sqrt{N_T}} [1, e^{j\frac{2\pi}{\lambda} d \sin(\phi_l^T)}, ..., e^{j\frac{2\pi}{\lambda}(N_T-1) d \sin(\phi_l^T)}]^T.$$

The MIMO channel model in (9) can be compactly represented as

$$\mathbf{H}_{n,u} = \mathbf{A}_{R,n,u} \mathbf{H}_{n,u}^{\beta} \mathbf{A}_{T,n,u}^H, \quad (10)$$

where $\mathbf{A}_T = [\mathbf{a}_T(\phi_{l,n,u}^T), ..., \mathbf{a}_T(\phi_{L,n,u}^T)] \in \mathbb{C}^{N_T \times L}$ and $\mathbf{A}_R = [\mathbf{a}_R(\phi_{l,n,u}^R), ..., \mathbf{a}_R(\phi_{L,n,u}^R)] \in \mathbb{C}^{N_R \times L}$ are the concatenated matrices of the transmit and receive array manifold vectors, respectively. The diagonal matrix $\mathbf{H}_{n,u}^{\beta} = \mathrm{diag}\left(\beta_{n,u}^{(1)}, \beta_{n,u}^{(2)}, ..., \beta_{n,u}^{(L)}\right)$ contains the path gains for each diagonal entry. Next, we determine the statistical properties of the ASI $\boldsymbol{\nu}_n^{(l,g)}(m)$. This study primarily focuses on single-carrier communication over flat-fading channels. However, there is potential for future research to substantially broaden its perspective to include delay-dispersive (frequency-selective) channels, with a particular emphasis on the widely used orthogonal frequency division multiplexing (OFDM) waveform.

B. Statistics of the asynchronous interference (ASI)

Observe from (5) that the expected value of ASI is zero, i.e., $\mathbb{E}[\boldsymbol{\nu}_n^{(l,g)}(m)] = 0$, for all l, g, and n, and $\mathbb{E}[\boldsymbol{\nu}_{n_1}^{(i,g)}(m)(\boldsymbol{\nu}_{n_2}^{(k,g)}(m))^H] = 0$, for user groups $i \neq k$, $i \neq g$, and $k \neq g$ and APs n_1 and n_2. Let the cross-covariance for $i = k = l \neq g$ between $\boldsymbol{\nu}_{n_1}^{(l,g)}(m)$ and $\boldsymbol{\nu}_{n_2}^{(l,g)}(m)$ be defined as

$$\mathbb{E}[\boldsymbol{\nu}_{n_1}^{(l,g)}(m) \boldsymbol{\nu}_{n_2}^{(l,g)}(m)^H] = \alpha_{n_1,n_2}^{(l,g)} \mathbf{I}_K, \quad (11)$$

where the quantity $\alpha_{n_1,n_2}^{(l,g)}$ denotes the asynchronous interference correlation, which can be formulated as [17], [42]

$$\alpha_{n_1,n_2}^{(l,g)} = \begin{cases} 0, & \text{if } \left| m_{n_2}^{(l,g)} - m_{n_1}^{(l,g)} \right| \geq 1; \\ \rho\left(\delta_{n_1}^{(l,g)}\right) \rho\left(\delta_{n_2}^{(l,g)} - T\right), & \text{if } m_{n_2}^{(l,g)} = m_{n_1}^{(l,g)} + 1; \\ \rho\left(\delta_{n_1}^{(l,g)} - T\right) \rho\left(\delta_{n_2}^{(l,g)} - T\right) + \rho\left(\delta_{n_1}^{(l,g)}\right) \rho\left(\delta_{n_2}^{(l,g)}\right), & \text{if } m_{n_2}^{(l,g)} = m_{n_1}^{(l,g)}; \\ \rho\left(\delta_{n_2}^{(l,g)}\right) \rho\left(\delta_{n_1}^{(l,g)} - T\right), & \text{if } m_{n_2}^{(l,g)} = m_{n_1}^{(l,g)} - 1. \end{cases} \quad (12)$$

Also, $\alpha_{n_1,n_2}^{(g,g)} = 1$, for all APs n_1 and n_2. Since all the U users employ an identical waveform, the correlation values of the ASI associated with different timing parameters can be computed in advance and stored in a look-up table. Furthermore, note that we have considered both line-of-sight (LoS) and non-LoS (NLoS) components to model the ASI. It is important to note that the system model of Section II represents a multicast framework, wherein a user group can make requests for identical information. A specific instance of this multicast information transmission is the unicast scenario, where each user requests distinct data, as described in the next section.

III. Precoder/ Combiner Design for Unicast Scenarios

This section designs the BB TPs and RCs for a mmWave unicast scenario, wherein each user requests different services. Thus, there is a single user in each group, i.e., $G = U$ and $U_g = 1$, where U represents the total number of users present in the system. The signal $\tilde{\mathbf{r}}_u(m) \in \mathbb{C}^{N_{\mathrm{RF},u} \times 1}$ received at user u, after RF combining at time index m, can be expressed as

$$\tilde{\mathbf{r}}_u(m) = \sum_{n=1}^{N} \mathbf{W}_{\mathrm{RF,u}}^H \mathbf{H}_{u,n} \mathbf{F}_{\mathrm{RF,n}} \mathbf{F}_{\mathrm{BB},u,n} \mathbf{x}_u(m) + \sum_{\substack{j=1 \\ j \neq u}}^{U} \sum_{n=1}^{N} \mathbf{W}_{\mathrm{RF,u}}^H \mathbf{H}_{u,n} \mathbf{F}_{\mathrm{RF,n}} \mathbf{F}_{\mathrm{BB,j,n}} \boldsymbol{\nu}_{ju,n}(m) + \mathbf{W}_{\mathrm{RF},u}^H \tilde{\mathbf{v}}_u(m), \quad (13)$$

where $\mathbf{x}_u(m)$ represents the signal vector intended for user u and $\tilde{\mathbf{v}}_u(m) \in \mathbb{C}^{N_R \times 1}$ denotes the AWGN vector at the uth user. One can design the RF TP and RC as follows: set the columns of the RF TP $\mathbf{F}_{\mathrm{RF},n}$ as the dominant $N_{\mathrm{RF},n}$ transmit array manifold vectors corresponding to each user. In a similar manner, the columns of the RF RC $\mathbf{W}_{\mathrm{RF},u}$ can be selected as the $N_{\mathrm{RF},u}$ dominant receive array manifold vectors corresponding to each AP. Initially, one can obtain the index $\mathcal{I}_{u,n}$ of the multipath component associated with the user u that has the maximum absolute path gain, i.e., $\mathcal{I}_{u,n} = \max\left\{\left|\beta_{u,n}^{(l)}\right|, \left|\beta_{u,n}^{(2)}\right|, \ldots, \left|\beta_{u,n}^{(L)}\right|\right\}$, to design the RF TP for the nth AP. The RF TP $\mathbf{F}_{\mathrm{RF},n}$ for the nth AP can now be obtained by selecting the $N_{\mathrm{RF},n}$ columns indexed by the set $\mathcal{I}_n = \{\mathcal{I}_{1,n}, \mathcal{I}_{2,n}, \ldots, \mathcal{I}_{U,n}\}$ from the matrix $\mathbf{A}_{T,u,n}$. This can be mathematically represented as

$$\mathbf{F}_{\mathrm{RF},n} = \left[\mathbf{A}_{T,1,n}(:, \mathcal{I}_{1,n}), \ldots, \mathbf{A}_{T,U,n}(:, \mathcal{I}_{U,n})\right]. \quad (14)$$

In a similar fashion, one can also obtain the RF RC $\mathbf{W}_{\mathrm{RF},u}$ for each user. Let $\tilde{\mathbf{H}}_{u,n} = \mathbf{W}_{\mathrm{RF,u}}^H \mathbf{H}_{u,n} \mathbf{F}_{\mathrm{RF},n} \in \mathbb{C}^{N_{\mathrm{RF},u} \times N_{\mathrm{RF},n}}$ denote the effective end-to-end channel matrix from the nth AP to the uth user. Furthermore, let us define the concatenated end-to-end channel matrix $\tilde{\mathbf{H}}_u \in \mathbb{C}^{N_{\mathrm{RF},u} \times \tilde{N}}$ containing the channels spanning from the uth user to all the APs and the corresponding stacked BB TP matrix $\mathbf{F}_{\mathrm{BB},u} \in \mathbb{C}^{\tilde{N} \times K}$ of the uth user as $\tilde{\mathbf{H}}_u = \left[\mathbf{W}_{\mathrm{RF},u}^H \mathbf{H}_{u,1} \mathbf{F}_{\mathrm{RF},1}, ..., \mathbf{W}_{\mathrm{RF},u}^H \mathbf{H}_{u,N} \mathbf{F}_{\mathrm{RF},N}\right]$ and $\mathbf{F}_{\mathrm{BB},u} = \left[\mathbf{F}_{\mathrm{BB},u,1}^T, \ldots, \mathbf{F}_{\mathrm{BB},u,N}^T\right]^T$, respectively. Upon employing the BB RC $\mathbf{W}_{\mathrm{BB,u}} \in \mathbb{C}^{N_{\mathrm{RF},u} \times K}$, the combined output signal at user u can be expressed as

$$\begin{aligned}\mathbf{r}_u(m) &= \mathbf{W}_{\mathrm{BB},u}^H \tilde{\mathbf{H}}_u \mathbf{F}_{\mathrm{BB},u} \mathbf{x}_u(m) \\ &+ \sum_{j \neq u}^{U} \sum_{n=1}^{N} \mathbf{W}_{\mathrm{BB},u}^H \tilde{\mathbf{H}}_{u,n} \mathbf{F}_{\mathrm{BB},j} \boldsymbol{\nu}_{ju,n}(m) + \mathbf{v}_u(m), \quad (15)\end{aligned}$$

where $\mathbf{v}_u(m) = \mathbf{W}_{\mathrm{BB},u}^H \mathbf{W}_{\mathrm{RF,u}}^H \tilde{\mathbf{v}}_u(m)$. Let $\boldsymbol{\nu}_{ju,n}(m)$ represent the ASI experienced by the uth user due to the signal transmitted by the nth AP intended for user j, which is defined as

$$\boldsymbol{\nu}_{ju,n}(m) = \rho(\delta_{ju,n} - T)\mathbf{x}_j(m_{ju,n}) + \rho(\delta_{ju,n})\mathbf{x}_j(m_{ju,n}+1).$$

Our goal is to design the BB TP and RC matrices for cell-free mmWave MIMO networks to mitigate the ASI. However, obtaining the linear TP and RC in the absence of ASI is a conceptually complex and computationally challenging task. In the presence of ASI, the conventional ZF methods [23], [43], which design the TP/RC matrices by satisfying the constraints, $\tilde{\mathbf{H}}_u \mathbf{F}_{\mathrm{BB},j} = 0$, $\forall\ u \neq j$, cannot eliminate all the interference terms in (7). Furthermore, it has been demonstrated that the ZF methods are capable of supporting only $U \leq \frac{\sum_{n=1}^{N} N_{\mathrm{RF},n}}{N_{\mathrm{RF},u}}$ users, imposing a significant undesirable constraint [34]. Note that this constraint arises only in the ZF TP/RC, since it tries to completely cancel the multi-user interference. By contrast, the proposed WHB and SHB schemes minimize and maximize the NMSE and SLNR, respectively, thus not imposing any constraint. The WHB and SHB have been considered as the TP/RC design methods in the proposed work for a cell-free mmWave MIMO network to mitigate the ASI. These two methods offer the benefit of being analytically tractable. Thus, we shall compare them in terms of their enhancements of the individual metrics and their collective impact on the capacity of the system. The next section develops the WHB technique for designing the TPs/RCs for cooperative cell-free mmWave MIMO systems.

A. Wiener hybrid beamforming for unicast scenarios

In this method, the goal is to jointly design the BB TPs $\{\mathbf{F}_{\mathrm{BB},u}\}_{u=1}^{U}$ and RCs $\{\mathbf{W}_{\mathrm{BB},u}\}_{u=1}^{U}$ of all the U users by minimizing the NMSE between the desired signal $\mathbf{d}_u$ and the received signal $\mathbf{r}_u$. The advantage of using this method is that it optimizes the system performance at both the transmitter and receiver end. The desired signal $\mathbf{d}_u$ is processed to imitate a single-user MIMO scenario in which it is devoid of noise and inter-user interference. The ideal desired signal can therefore be set as $\mathbf{d}_u = \tilde{\mathbf{H}}_u \mathbf{B}_u \mathbf{x}_u$. The linear TP matrix $\mathbf{B}_u$ can be obtained by the eigenvalue decomposition of the channel matrix $\tilde{\mathbf{H}}_u$, followed by power allocation using the water-filling strategy that maximizes the capacity of the system in the interference-free scenario. The NMSE is defined as

$$\mathrm{NMSE} = \sum_{u=1}^{U} \frac{\mathbb{E}[\|\mathbf{r}_u - \mathbf{d}_u\|^2]}{\Omega_u} = \sum_{u=1}^{U} \mathrm{NMSE}_u, \quad (16)$$

where $\mathrm{NMSE}_u = \frac{\mathbb{E}[\|\mathbf{r}_u - \mathbf{d}_u\|^2]}{\Omega_u}$ denotes the NMSE of the uth user and $\Omega_u = \mathbb{E}[\mathrm{Tr}\left\{\mathbf{d}_u \mathbf{d}_u^H\right\}] = \mathrm{Tr}\left\{\tilde{\mathbf{H}}_u \mathbf{B}_u \mathbf{B}_u^H \tilde{\mathbf{H}}_u^H\right\}$ represents the average received power of the desired signal. Let $\mathbf{J}_u = \sum_{j \neq u}^{U} \sum_{n=1}^{N} \mathbf{W}_{\mathrm{BB},u}^H \tilde{\mathbf{H}}_{u,n} \mathbf{F}_{\mathrm{BB},j,n} \boldsymbol{\nu}_{ju,n}(m)$ denote the multi-user interference term in (15). Thus, the NMSE expression of the uth user can be formulated as

$$\begin{aligned}\mathrm{NMSE}_u = \frac{1}{\Omega_u} \mathbb{E}\Big[&\left(\mathbf{W}_{\mathrm{BB},u}^H \tilde{\mathbf{H}}_u \mathbf{F}_{\mathrm{BB},u} \mathbf{s}_u - \mathbf{A}_u \mathbf{s}_u + \mathbf{J}_u + \mathbf{v}_u\right)^H \\ &\left(\mathbf{W}_{\mathrm{BB},u}^H \tilde{\mathbf{H}}_u \mathbf{F}_{\mathrm{BB},u} \mathbf{s}_u - \mathbf{A}_u \mathbf{s}_u + \mathbf{J}_u + \mathbf{v}_u\right)\Big], \quad (17)\end{aligned}$$

where $\mathbf{A}_u = \tilde{\mathbf{H}}_u \mathbf{B}_u$. Upon employing the results obtained in Section II-B, the simplified NMSE_u expression can be obtained as shown in (18). The cooperative TP and RC design problem of mitigating the ASI, which minimizes the total NMSE while satisfying the power constraint, can be formulated as

$$\begin{aligned}&\min_{\{\mathbf{W}_{\mathrm{BB,u}}\}_{u=1}^{U}, \{\mathbf{F}_{\mathrm{BB,u}}\}_{u=1}^{U}} \sum_{u=1}^{U} \mathrm{NMSE}_u \\ &\text{s.t.} \quad \mathrm{Tr}\left\{(\mathbf{F}_{\mathrm{BB},u})^H \mathbf{F}_{\mathrm{BB},u}\right\} \leq P_u, \quad \forall u. \quad (19)\end{aligned}$$

To obtain the solution for the cooperative beamformer, we minimize the following Lagrangian constructed for the above problem:

$$\mathrm{NMSE}_u = \frac{1}{\Omega_u}\mathrm{Tr}\left\{\sum_{n_1=1}^{N}\sum_{n_2=1}^{N}\mathbf{W}_{\mathrm{BB},u}^H\tilde{\mathbf{H}}_{u,n_1}\mathbf{F}_{\mathrm{BB},u,n_1}\mathbf{F}_{\mathrm{BB},u,n_2}^H\mathbf{H}_{\mathrm{BB},u,n_2}^H\mathbf{W}_{\mathrm{BB},u}\right\} - \frac{1}{\Omega_u}\mathrm{Tr}\left\{\sum_{n=1}^{N}\mathbf{W}_{\mathrm{BB},u}^H\tilde{\mathbf{H}}_{u,n}\mathbf{F}_{\mathrm{BB},u,n}\mathbf{A}_u^H\right\}$$
$$+ \frac{1}{\Omega_u}\mathrm{Tr}\left\{-\mathbf{A}_u\sum_{n=1}^{N}\mathbf{F}_{\mathrm{BB},u}^H\tilde{\mathbf{H}}_{u,n}^H\mathbf{W}_{\mathrm{BB},u} + \mathbf{A}_u\mathbf{A}_u^H\right\} + \frac{1}{\Omega_u}\mathrm{Tr}\left\{\mathbf{W}_{\mathrm{BB},u}^H\mathbf{W}_{\mathrm{RF},u}^H\mathbf{W}_{\mathrm{RF},u}\mathbf{W}_{\mathrm{BB},u}\right\}$$
$$+ \frac{1}{\Omega_u}\mathrm{Tr}\left\{\sum_{j\neq k}^{K}\sum_{n_1=1}^{N}\sum_{n_2=1}^{N}\alpha_{ju,n_1,n_2}\mathbf{W}_{\mathrm{BB},u}^H\tilde{\mathbf{H}}_{u,n_1}\mathbf{F}_{\mathrm{BB},j,n_1}\mathbf{F}_{\mathrm{BB},j,n_2}^H\tilde{\mathbf{H}}_{u,n_2}^H\mathbf{W}_{\mathrm{BB},u}\right\}, \tag{18}$$

$$f\left(\{\mathbf{F}_{\mathrm{BB},u},\mathbf{W}_{\mathrm{BB},u}\}_{u=1}^{U}\right) = \sum_{u=1}^{U}\mathrm{NMSE}_u + \sum_{u=1}^{U}\zeta_u\left(\mathrm{Tr}\left\{\sum_{n=1}^{N}(\mathbf{F}_{\mathrm{BB},u,n})^H\mathbf{F}_{\mathrm{BB},u,n}\right\} - P_u\right), \tag{20}$$

where ζ_u denotes the Lagrange multiplier associated with the power constraints for the uth user and $\mathrm{Tr}\left\{\sum_{n=1}^{N}(\mathbf{F}_{\mathrm{BB},u,n})^H\mathbf{F}_{\mathrm{BB},u,n}\right\} = \mathrm{Tr}\left\{(\mathbf{F}_{\mathrm{BB},u})^H\mathbf{F}_{\mathrm{BB},u}\right\}$. Solving (20) by applying the KKT conditions [44] with respect to the variable matrices, i.e. the optimal BB TP $\mathbf{F}_{\mathrm{BB},u,n}$ and RC $\mathbf{W}_{\mathrm{BB},u}$, these quantities can be derived as shown below. To begin with, $\mathbf{F}_{\mathrm{BB},u,n}$ is determined as

$$\mathbf{F}_{\mathrm{BB},u} = \frac{1}{\Omega_u}(\mathbf{C}_u + \zeta_u\mathbf{I}_{\tilde{N}})^{-1}\tilde{\mathbf{H}}_u^H\mathbf{W}_{\mathrm{BB},u}\mathbf{A}_u, \tag{21}$$

where the matrix $\mathbf{C}_u$ and its components $\mathbf{C}_{u,n_1,n_2}$ are defined as

$$\mathbf{C}_u = \begin{bmatrix}\mathbf{C}_{u,1,1} & \mathbf{C}_{u,1,2} & \cdots & \mathbf{C}_{u,1,N}\\ \mathbf{C}_{u,2,1} & \mathbf{C}_{u,2,2} & \cdots & \mathbf{C}_{u,2,N)}\\ \vdots & \vdots & \ddots & \vdots\\ \mathbf{C}_{u,N,1} & \mathbf{C}_{u,N,2} & \cdots & \mathbf{C}_{u,N,N}\end{bmatrix}, \tag{22}$$

$$\mathbf{C}_{u,n_1,n_2} = \sum_{j=1}^{U}\frac{\alpha_{n_1,n_2}^{(u,j)}}{\Omega_j}\tilde{\mathbf{H}}_{j,n_1}^H\mathbf{W}_{\mathrm{BB},u}\mathbf{W}_{\mathrm{BB},u}^H\tilde{\mathbf{H}}_{j,n_2}. \tag{23}$$

The quantity $\mathbf{W}_{\mathrm{BB},u}$ can be expressed as

$$\mathbf{W}_{\mathrm{BB},u} = \frac{1}{\Omega_u}\left(\mathbf{G}_u + \mathbf{W}_{\mathrm{RF},u}^H\mathbf{W}_{\mathrm{RF},u}\right)^{-1}\tilde{\mathbf{H}}_u\mathbf{F}_{\mathrm{BB},u}\mathbf{A}_u, \tag{24}$$

where the matrix $\mathbf{G}_u$ is defined similar to $\mathbf{C}_u$ in (22) and the sub-matrix $\mathbf{G}_{u,n_1,n_2}$ is formulated as

$$\mathbf{G}_{u,n_1,n_2} = \sum_{j=1}^{U}\frac{\alpha_{n_1,n_2}^{(u,j)}}{\Omega_j}\tilde{\mathbf{H}}_{j,n_1}^H\mathbf{F}_{\mathrm{BB},j,n_1}\mathbf{F}_{\mathrm{BB},j,n_2}^H\tilde{\mathbf{H}}_{j,n_2}. \tag{25}$$

The key aspect of the WHB-based hybrid design is that both the BB TP $\mathbf{F}_{\mathrm{BB},u}$ and RC $\mathbf{W}_{\mathrm{BB},u}$ incorporate the effect of ASI. Since the optimum BB TPs $\{\mathbf{F}_{\mathrm{BB},u}\}_{u=1}^{U}$ and RCs $\{\mathbf{W}_{\mathrm{BB},u}\}_{u=1}^{U}$ are interdependent, direct computation of these quantities is mathematically intractable. To circumvent this challenge, we propose a WHB algorithm that iteratively designs the TPs and RCs. At each iteration, the algorithm initially evaluates each $\mathbf{F}_{\mathrm{BB},u}$ for a given $\mathbf{W}_{\mathrm{BB},u}$ and subsequently updates $\mathbf{W}_{\mathrm{BB},u}$ using (24) for a fixed $\mathbf{F}_{\mathrm{BB},u}$. The iterative nature of the WHB algorithm also leads to improved alignment of the RCs at the users with the TPs at the AP, and vice versa. The iterative nature of the WHB algorithm also enables the RCs at the users to better align with the TPs at the AP, and vice versa in comparison to the works [35]–[37] that only design fully digital TP or RC. A step-by-step procedure describing the WHB-based TP and RC design procedure is presented in Algorithm 1. Next, we conceived an alternative method for the design of the cooperative ASI cancellation beamformer considering the SLNR criterion, which is presented next.

Algorithm 1: WHB procedure

1 **Input:** $\tilde{\mathbf{H}}_u$, $\mathbf{W}_{\mathrm{RF},u}$, $\alpha_{n_1,n_2}^{(u,j)}$, stopping parameter υ;
2 **Initialization:** $\mathbf{W}_{\mathrm{BB},u}^{(0)}$, set counter $k=0$;
3 **while** $\left(\left\|\mathbf{W}_{\mathrm{BB},u}^{(k+1)} - \mathbf{W}_{\mathrm{BB},u}^{(k)}\right\|_F^2 > \upsilon\right)$ **do**
  i **TP-step:** Compute the matrices $\{\mathbf{F}_{\mathrm{BB},u}^{(k)}\}_{u=1}^{U}$ using (21).
  ii **RC-step:** Use $\{\mathbf{F}_{\mathrm{BB},u}^{(k)}\}_{u=1}^{U}$ updated in TCP-step to compute $\{\mathbf{W}_{\mathrm{BB},u}^{(k)}\}_{u=1}^{U}$ using (24).
  end
4 **Output:** $\{\mathbf{F}_{\mathrm{BB},u}\}_{u=1}^{U}$ and $\{\mathbf{W}_{\mathrm{BB},u}\}_{u=1}^{U}$.

B. SLNR-based hybrid beamforming for unicast scenarios (SHB-U)

In this method, we consider SLNR as a performance metric for designing the hybrid beamformer. The SLNR refers to the ratio of the power of the desired signal received at the uth user and the sum of the noise plus the total interference power (leakage) at other users due to the transmission to the uth user. On the other hand, the SINR is defined as the ratio of desired signal power and the sum of interference plus noise power at user u. No closed-form solutions are available for maximizing the SINR due to the coupled nature of the optimization problem. The solution obtained by maximizing the SLNR is sub-optimal compared to the SINR metric because it only tries to maximize the SLNR from the transmitter's perspective and cannot guarantee SINR maximization at the receiver end. However, the SLNR metric provides a closed-form expression for

TPs and RCs, and we show that the largest value that the SLNR ratio can achieve is equal to the maximum eigenvalue of a certain matrix. The SHB-U scheme designs the BB TP $\mathbf{F}_{\mathrm{BB},u}$ of all the users via the maximization of the SLNR. The SHB-U scheme minimizes the interference that is caused by the signal transmission to a user rather than the interference at the receiver of the user. While designing the BB TPs for each user, we restrict the search space to matrices of the form $\mathbf{F}_{\mathrm{BB},u} = \sqrt{\frac{P_u}{K}}\mathbf{Q}_u$, where the matrix $\mathbf{Q}_u \in \mathbb{C}^{\tilde{N}\times K}$ is a semi-unitary matrix, i.e., $\mathbf{Q}_u^H\mathbf{Q}_u = \mathbf{I}_K$. Although this restriction leads to sub-optimality, it results in a manageable framework for the computation of the BB TPs as the solution to the pertinent SLNR maximization problem. Interestingly, this also leads to enhanced performance, since the orthonormality eliminates the interference among the streams received at the user.

We commence by deriving the expression for the SLNR. The desired signal component received by the uth user is $\mathbf{x}_u = \sqrt{\frac{P_u}{K}}\tilde{\mathbf{H}}_u\mathbf{Q}_u\mathbf{s}_u$ and the corresponding desired signal power is $P_{R,u} = \frac{P_u}{K}\mathrm{Tr}\left\{\mathbf{Q}_u^H\tilde{\mathbf{H}}_u^H\tilde{\mathbf{H}}_u\mathbf{Q}_u\right\}$. Based on (15), the ASI leakage at user j due to the signal x_u intended for user u, transmitted by the N APs, is expressed as $\sum_{n=1}^{N}\tilde{\mathbf{H}}_{j,n}\mathbf{F}_{\mathrm{BB},u,n}\boldsymbol{\nu}_{uj,n}$. Therefore, the power of this leakage signal P_{uj}^L is given by

$$P_{uj}^L = \frac{P_u}{K}\sum_{n_1=1}^{N}\sum_{n_2=1}^{N}\alpha_{n_1,n_2}^{u,j}\mathrm{Tr}\Big\{\mathbf{Q}_{u,n_1}^H\tilde{\mathbf{H}}_{j,n_1}^H\tilde{\mathbf{H}}_{j,n_2}^H\mathbf{Q}_{u,n_2}\Big\},$$

where the sub-matrix $\mathbf{Q}_{u,n}$ accumulates the rows in the matrix Q_u corresponding to the nth AP. Note that the noise power at the uth user is $\sigma^2\mathrm{Tr}\left\{\mathbf{W}_{\mathrm{RF},u}^H\mathbf{W}_{\mathrm{RF},u}\right\}$. Therefore, the expression of the SLNR for user u can be expressed as

$$\mathrm{SLNR}_u = \frac{P_{R,u}}{\sum_{j\neq u}^{U}P_{uj}^L + \sigma^2\mathrm{Tr}\left\{\mathbf{W}_{\mathrm{RF},u}^H\mathbf{W}_{\mathrm{RF},u}\right\}}. \quad (26)$$

Moreover, one can simplify the SLNR_u expression as

$$\mathrm{SNLR}_u = \frac{\mathrm{Tr}\left\{(\mathbf{Q}_u)^H\mathbf{T}_u\mathbf{Q}_u\right\}}{\mathrm{Tr}\left\{(\mathbf{Q}_u)^H\mathbf{R}_u\mathbf{Q}_u\right\}} = \frac{\sum_{k=1}^{K}\mathbf{q}_{uk}^H\mathbf{T}_u\mathbf{q}_{uk}}{\sum_{k=1}^{K}\mathbf{q}_{uk}^H\mathbf{R}_u\mathbf{q}_{uk}}, \quad (27)$$

where q_{uk} represents the kth column of the matrix $\mathbf{Q}_u$, $\mathbf{T}_u = P_u\tilde{\mathbf{H}}_u^H\tilde{\mathbf{H}}_u$ and $\mathbf{R}_u = \sigma^2\mathbf{W}_{\mathrm{RF},u}^H\mathbf{W}_{\mathrm{RF},u} + \sum_{j\neq u}^{U}P_u\mathbf{Z}_{uj}$. The quantity $\mathbf{Z}_{uj} \in \mathbb{C}^{\tilde{N}\times\tilde{N}}$ is constructed as

$$\mathbf{Z}_{uj} = \begin{bmatrix} \alpha_{1,1}^{(u,j)}\tilde{\mathbf{H}}_{j,1}^H\tilde{\mathbf{H}}_{j,1} & \cdots & \alpha_{1,N}^{(u,j)}\tilde{\mathbf{H}}_{j,1}^H\tilde{\mathbf{H}}_{j,N} \\ \alpha_{2,1}^{(u,j)}\tilde{\mathbf{H}}_{j,2}^H\tilde{\mathbf{H}}_{j,1} & \cdots & \alpha_{2,N}^{(u,j)}\tilde{\mathbf{H}}_{j,2}^H\tilde{\mathbf{H}}_{j,N} \\ \vdots & \ddots & \vdots \\ \alpha_{N,1}^{(u,j)}\tilde{\mathbf{H}}_{j,N}^H\tilde{\mathbf{H}}_{j,1} & \cdots & \alpha_{N,N}^{(u,j)}\tilde{\mathbf{H}}_{j,N}^H\tilde{\mathbf{H}}_{j,N} \end{bmatrix}. \quad (28)$$

One can note that the optimization problem constructed for obtaining the cooperative BB TP by maximizing the SLNR can be decomposed into decoupled problems for different users, as shown in [45]. Thus, the optimization problem of the cooperative BB TP design for user u can be expressed as

$$\mathbf{Q}_u^{\mathrm{opt}} = \arg\max_{\mathbf{Q}_u}\mathrm{SLNR}_u, \quad \forall u. \quad (29)$$

However, designing the cooperative TPs for different users to determine the optimal quantities $\mathbf{q}_{kl}, \cdots, \mathbf{q}_{uLu}$ is still mathematically intractable. To overcome this challenge, we consider a lower bound for the quantity SLNR_u, which is expressed as

$$\mathrm{SLNR}_u \geq \min_{k=1,\ldots,K}\frac{(\mathbf{q}_{uk})^H\mathbf{T}_u\mathbf{q}_{uk}}{(\mathbf{q}_{uk})^H\mathbf{R}_u\mathbf{q}_{uk}}. \quad (30)$$

Observe that maximizing the lower bound in (30) on the SLNR for the user u leads to the maximization of the minimum generalized Rayleigh-Ritz quotient among all its signal streams. Thus, the optimal matrix $\mathbf{Q}_u^{\mathrm{opt}}$ which maximizes the SLNR_u for the uth user can be obtained by solving the following max-min optimization problem

$$\mathbf{Q}_u^{\mathrm{opt}} = \arg\max_{\mathbf{Q}_u:\,\mathbf{Q}_u^H\mathbf{Q}_u=\mathbf{I}_K}\min_{k=1,\ldots,K}\frac{\mathbf{q}_{uk}^H\mathbf{T}_u\mathbf{q}_{uk}}{\mathbf{q}_{uk}^H\mathbf{R}_u\mathbf{q}_{uk}}. \quad (31)$$

Note that the lower bound in expression (30) for SLNR_u is maximized when

$$\mathbf{q}_{uk}^{\mathrm{opt}} = \mathbf{v}_k(\mathbf{R}_u^{-1}\mathbf{T}_u), \quad \forall k, \quad (32)$$

where $\mathbf{v}_k(\mathbf{R}_u^{-1}\mathbf{T}_u)$ denotes the eigenvector corresponding to the kth largest eigenvalue of the matrix $\mathbf{R}_u^{-1}\mathbf{T}_u$. Thus, the BB TP of user u can now be obtained by stacking the columns $\mathbf{q}_{uk}^{\mathrm{opt}}$ across all the K streams, i.e., $\mathbf{F}_{\mathrm{BB},u} = \sqrt{\frac{P_u}{K}}\left[\mathbf{q}_{u1}^{\mathrm{opt}}\mathbf{q}_{u2}^{\mathrm{opt}}\cdots\mathbf{q}_{uK}^{\mathrm{opt}}\right]$. The corresponding BB RC can be computed as the MMSE combiner using (24). One can observe that the SHB-based TP in (32) is a function of not only the channel matrix but also of the asynchronous interference. The SLNR performance metric is considered in [40] for mmWave massive MIMO systems for a single AP, $K = 1$ stream, and RA at each user. However, the framework proposed in [40] failed to incorporate the ASI.

IV. Hybrid Precoder/ Combiner Design for Multicast Scenarios

As discussed in Section II, the users belonging to the same group of a multicast scenario request identical data. For such a system, one can formulate the joint Wiener filtering method and joint leakage suppression techniques for designing the hybrid TPs and RCs, similar to JHB-U and SHB-U derived for the unicast scenario, that successfully minimizes the overall normalized MSE and maximizes the SLNR, respectively. As described in Section II, after RF and

BB combining, the signal $\tilde{\mathbf{y}}^{(g)}(m) = \left(\mathbf{W}_{\mathrm{BB},u}^{(g)}\right)^H \mathbf{y}^{(g)}(m)$ received by the uth user of the group g, can be expressed as

$$\begin{aligned}\mathbf{r}_u^{(g)}(m) &= \left(\mathbf{W}_{\mathrm{BB},u}^{(g)}\right)^H \tilde{\mathbf{H}}_u^{(g)} \mathbf{F}_{\mathrm{BB}}^{(g)} \mathbf{x}^{(g)}(m) \\ &+ \left(\mathbf{W}_{\mathrm{BB},u}^{(g)}\right)^H \sum_{\substack{l=1 \\ l\neq g}}^{G} \sum_{n=1}^{N} \tilde{\mathbf{H}}_{u,n}^{(g)} \mathbf{F}_{\mathrm{BB},n}^{(l)} \boldsymbol{\nu}_n^{(l,g)}(m) \\ &+ \left(\mathbf{W}_{\mathrm{BB},u}^{(g)}\right)^H \mathbf{v}_u^{(g)}(m). \end{aligned} \tag{33}$$

Thus, the concatenated received signal across all the users of the gth group at the mth time instant is expressed as

$$\begin{aligned}\mathbf{r}^{(g)}(m) &= \left(\mathbf{W}_{\mathrm{BB}}^{(g)}\right)^H \tilde{\mathbf{H}}^{(g)} \mathbf{F}_{\mathrm{BB}}^{(g)} \mathbf{x}^{(g)}(m) \\ &+ \left(\mathbf{W}_{\mathrm{BB}}^{(g)}\right)^H \sum_{l\neq g}^{G} \sum_{n=1}^{N} \tilde{\mathbf{H}}_n^{(g)} \mathbf{F}_{\mathrm{BB},n}^{(l)} \boldsymbol{\nu}_n^{(l,g)}(m) + \tilde{\mathbf{v}}^{(g)}(m), \end{aligned} \tag{34}$$

where $\mathbf{W}_{\mathrm{BB}}^{(g)} = \mathrm{blkdiag}\left(\mathbf{W}_{\mathrm{BB},1}^{(g)}, \mathbf{W}_{\mathrm{BB},2}^{(g)}, \ldots, \mathbf{W}_{\mathrm{BB},U_g}^{(g)}\right)$ denotes a block-diagonal RC for the gth user group, where the various quantities above are defined as

$$\mathbf{r}^{(g)}(m) = \begin{bmatrix} \mathbf{r}_1^{(g)}(m) \\ \mathbf{r}_1^{(g)}(m) \\ \vdots \\ \mathbf{r}_{U_g}^{(g)}(m) \end{bmatrix}, \tilde{\mathbf{H}}^{(g)} = \begin{bmatrix} \tilde{\mathbf{H}}_1^{(g)} \\ \tilde{\mathbf{H}}_2^{(g)} \\ \vdots \\ \tilde{\mathbf{H}}_{U_g}^{(g)} \end{bmatrix}, \text{and}$$

$$\tilde{\mathbf{v}}^{(g)}(m) = \left[\left(\mathbf{W}_{\mathrm{BB},1}^{(g)}\right)^H \mathbf{v}_1^{(g)}, \cdots, \left(\mathbf{W}_{\mathrm{BB},U_g}^{(g)}\right)^H \mathbf{v}_{U_g}^{(g)}\right]^T.$$

Next, we describe the WHB and SHB frameworks for a multicast scenario.

A. Wiener hybrid beamforming for multicast (WHB-M)

Similar to the WHB-U algorithm of Section III-A, the goal of the scheme presented in this section is to optimize the TPs $\{\mathbf{F}_{\mathrm{BB},g}\}_{g=1}^G$ and RCs $\left\{\mathbf{W}_{\mathrm{BB},u}^{(g)}\right\}_{g=1}^G$ that minimize the NMSE between the desired signals and the respective received signals over all the G groups. Let $\mathbf{d}^{(g)} = \tilde{\mathbf{H}}^{(g)}\mathbf{B}^{(g)}\mathbf{x}^{(g)}$ represent the desired received signal similar to Section III-A. The NMSE expression for the multicast scenario can be formulated as

$$\mathbf{NMSE} = \sum_{g=1}^{G} \frac{\mathbb{E}[\left\|\mathbf{r}^{(g)} - \mathbf{d}^{(g)}\right\|^2]}{\Omega^{(g)}} = \sum_{g=1}^{G} \mathbf{NMSE}^{(g)} \tag{35}$$

where $\Omega^{(g)} = \mathbb{E}[\mathbf{Tr}\left\{\mathbf{d}^{(g)}\mathbf{d}^{(g)H}\right\}] = \mathbf{Tr}\left\{\tilde{\mathbf{H}}^{(g)}\mathbf{B}^{(g)}(\mathbf{B}^{(g)})^H(\tilde{\mathbf{H}}^{(g)})\right\}$ denotes the average received power of the desired signal. Note that the expectation is taken over the symbols $\left\{\mathbf{x}^{(g)}\right\}_{g=1}^G$ and the noise $\left\{\mathbf{v}^{(g)}\right\}_{g=1}^G$. The NMSE optimization problem is then formulated as

$$\begin{aligned}\{\mathbf{F}_{\mathrm{BB}}^{(g)}\}_{g=1}^G &= \arg \min_{\{\mathbf{F}_{\mathrm{BB}}^{(g)}\}_{g=1}^G} \sum_{g=1}^{G} \mathrm{NMSE}^{(g)} \\ &\text{s.t. } \mathbf{Tr}\left\{(\mathbf{F}_{\mathrm{BB}}^{(g)})^H \mathbf{F}_{\mathrm{BB}}^{(g)}\right\} \leq P^{(g)}, \forall g. \end{aligned} \tag{36}$$

One can now employ the WHB-U framework given in Algorithm 1 for designing the TP/RC for this multicast scenario.

B. SLNR-based hybrid beamforming for multicast scenario (SHB-M)

Similar to the unicast scenario of Section III, the hybrid BB TPs are designed for the multicast scenario by maximizing the ratio between the desired signal power at the users in the gth group and the total interference leakage due to transmission to the gth group at all the other user groups, along with the noise. Once again, the TP for the gth group is considered to be of the form $\mathbf{F}_{\mathrm{BB}}^{(g)} = \sqrt{\frac{P^{(g)}}{K}}\mathbf{Q}^{(g)}$. The expression for the SLNR of gth group can be formulated as

$$\mathrm{SLNR}^{(g)} = \frac{\mathrm{Tr}\left\{(\mathbf{Q}^{(g)})^H \mathbf{M}^{(g)} \mathbf{Q}^{(g)}\right\}}{\mathrm{Tr}\left\{(\mathbf{Q}^{(g)})^H \mathbf{N}^{(g)} \mathbf{Q}^{(g)}\right\}} = \frac{\sum_{k=1}^{K^{(g)}} (\mathbf{q}_k^{(g)})^H \mathbf{M}^{(g)} \mathbf{q}_k^{(g)}}{\sum_{k=1}^{K^{(g)}} (\mathbf{q}_k^{(g)})^H \mathbf{N}^{(g)} \mathbf{q}_k^{(g)}}, \tag{37}$$

where $\mathbf{q}_k^{(g)}$ is the kth column of the matrix $\mathbf{Q}^{(g)}$. Therefore, the kth column of the optimal matrix $\mathbf{Q}_{\mathrm{opt}}^{(g)}$ is given by

$$\mathbf{q}_{\mathrm{opt},k}^{(g)} = \mathbf{v}_k\left(\mathbf{R}^{(g)^{-1}}\mathbf{T}^{(g)}\right), \quad \forall k, \tag{38}$$

where the matrices $\mathbf{R}^{(g)}$ and $\mathbf{T}^{(g)}$ are defined as $\mathbf{R}^{(g)} = \sigma^2 N_R \mathbf{W}_{\mathrm{RF}} + \sum_{\substack{l=1 \\ l\neq g}}^{G} P^{(g)} \mathbf{Z}^{(l,g)}$ and $\mathbf{T}^{(g)} = P^{(g)}(\tilde{\mathbf{H}}^{(g)})^H \tilde{\mathbf{H}}^{(g)}$, respectively, and

$$\mathbf{Z}^{(l,g)} = \begin{bmatrix} \alpha_{(1,1)}^{(l,g)} (\tilde{\mathbf{H}}_1^{(l)})^H \tilde{\mathbf{H}}_j^{(1)} & \cdots & \alpha_{(1,N)}^{(l,g)} (\tilde{\mathbf{H}}_1^{(l)})^H \tilde{\mathbf{H}}_j^{(N)} \\ \alpha_{(2,1)}^{(l,g)} \tilde{\mathbf{H}}_j^{(2)^H} \tilde{\mathbf{H}}_j^{(1)} & \cdots & \alpha_{(2,N)}^{(l,g)} (\mathbf{H}_{\mathrm{eff},j}^{(2)})^H \mathbf{H}_j^{(N)} \\ \vdots & \ddots & \vdots \\ \alpha_{(N,1)}^{(l,g)} (\tilde{\mathbf{H}}_N^{(l)})^H \tilde{\mathbf{H}}_j^{(1)} & \cdots & \alpha_{(N,N)}^{(l,g)} (\tilde{\mathbf{H}}_N^{(l)})^H \tilde{\mathbf{H}}_N^{(l)} \end{bmatrix}. \tag{39}$$

Next, we describe the BL-based hybrid TP/RC design, which does not require complete knowledge of the dominant array manifold vectors of the APs and users.

V. Bayesian learning based hybrid TP/RC design

Recall that the RF TP/RC design procedures described in the previous sections require prior knowledge of the array manifold vectors of the users and APs. This, in turn, necessitates prior information regarding the individual components of the mmWave MIMO channel, i.e., AoAs/AoDs and path gains of the multipath components. However, in the scenario when the individual components are unknown, and only an estimate of the channel matrix $\mathbf{H}_{u,n}$ is available, we propose a novel BL-based framework for designing the hybrid beamformer. Note that the proposed BL framework is capable of yielding superior performance in scenarios wherein the AoAs/AoDs and path gains are known, as well as those in which only an estimate of the channel matrix is available. In the case wherein prior information pertaining to the AoAs/AoDs is available, the size of the dictionary matrix

can be reduced by including the array steering vectors corresponding only to the known AoAs/AoDs. This in turn leads to a significant reduction in the computational complexity of the BL algorithm. For the challenging scenario wherein such prior information is not available, this section develops an innovative method of designing the hybrid TP/RC by decomposing the fully digital transceiver components obtained via the WHB and SHB schemes.

This section focuses on the joint design of the RF and BB TPs for a multicast scenario, but a similar approach can readily be formulated for a unicast scenario. Let $\mathbf{W}^{(g)} \in \mathbb{C}^{U_g N_R \times U_g K}$ denote the FD RC combiner defined similar to the BB RC in (34). The concatenated signal $\mathbf{r}^{(g)} \in \mathbb{C}^{U_g K \times 1}$ received at the gth group can be expressed as

$$\mathbf{r}^{(g)}(m) = \left(\mathbf{W}^{(g)}\right)^H \tilde{\mathbf{H}}^{(g)} \mathbf{F}^{(g)} \mathbf{x}^{(g)}(m) + \left(\mathbf{W}^{(g)}\right)^H \sum_{l \neq g}^{G} \sum_{n=1}^{N} \tilde{\mathbf{H}}_n^{(g)} \mathbf{F}_n^{(l)} \boldsymbol{\nu}_n^{(l,g)}(m) + \tilde{\mathbf{v}}^{(g)}(m), \quad (40)$$

where $\mathbf{F}^{(g)} \in \mathbb{C}^{NN_T \times K}$ denotes the stacked FD TP and the quantities $\mathbf{r}^{(g)}$, $\tilde{\mathbf{H}}^{(g)}$ and $\tilde{\mathbf{v}}^{(g)}(m)$ are defined in a fashion similar to (34). Let $\mathbf{F}_{\rm opt} = \left[\mathbf{F}_{\rm opt}^{(1)}, \mathbf{F}_{\rm opt}^{(2)}, \ldots, \mathbf{F}_{\rm opt}^{(G)}\right] \in \mathbb{C}^{NN_T \times KG}$ represent the concatenated FD TP for all the user groups obtained via employing the WHB-M or SHB-M frameworks, where $\mathbf{F}_{\rm opt}^{(g)} \in \mathbb{C}^{NN_T \times K}$ represents the FD TP for the gth user group. A BL-based design only requires knowledge about the mmWave MIMO channel matrices $\mathbf{H}_{u,m}$, but not the AoAs/AoDs or path gains of the multipath components. A BL-based procedure is now employed for decomposing the FD TP $\mathbf{F}_{\rm opt}$ into its BB $\mathbf{F}_{\rm BB}$ and RF $\mathbf{F}_{\rm RF}$ constituents. The optimization problem formulated for decoupling the FD TP can be expressed as

$$(\mathbf{F}_{\rm BB}^*, \mathbf{F}_{\rm RF}^*) = \underset{\mathbf{F}_{\rm BB}, \mathbf{F}_{\rm RF}}{\arg\min} \|\mathbf{F}_{\rm opt} - \mathbf{F}_{\rm RF}\mathbf{F}_{\rm BB}\|_{\rm F}^2 \quad \text{s.t.} \quad |\mathbf{F}_{\rm RF}(i,j)| = \frac{1}{\sqrt{N_T}}, \quad (41)$$

where $\mathbf{F}_{\rm BB} = \left[\mathbf{F}_{\rm BB}^{(1)}, \mathbf{F}_{\rm BB}^{(2)}, \ldots, \mathbf{F}_{\rm BB}^{(G)}\right] \in \mathbb{C}^{\tilde{N} \times KU}$ and $\mathbf{F}_{\rm RF} = \text{blkdiag}\left(\mathbf{F}_{\rm RF,1}, \ldots, \mathbf{F}_{\rm RF,n}\right) \in \mathbb{C}^{NN_T \times \tilde{N}}$ represents the concatenated BB TP of all the users and the block-diagonal matrix of the RF TPs corresponding to all the APs, respectively. Note that the problem in (41) is non-convex due to the constant-magnitude constraint imposed on each entry of the RF TPs, and it is hence mathematically intractable. To address this issue, we commence by defining a dictionary matrix of the feasible transmit array manifold vectors as $\mathbf{G}_T = \left[\mathbf{a}_T(\phi_1), \mathbf{a}_T(\phi_2), \cdots, \mathbf{a}_T(\phi_S)\right] \in \mathbb{C}^{N_T \times S}$, where the set of AoDs $\{\phi_s,\ \forall 1 \leq s \leq S\}$ spans the angular range $[0,\ \pi]$, obeying $\cos(\phi_s) = \frac{2}{S}(s-1) - 1$, and the quantity S represents the angular grid size [1]. It is important to observe that the each entry of the matrix $\mathbf{G}_T$ is adheres to the constraint of (41). Consequently, the columns of the RF TP $\mathbf{F}_{\rm RF}$ can be appropriately selected from the dictionary matrix $\mathbf{G}_T$. The corresponding problem formulated for our hybrid TP design can be recast as

$$\underset{\tilde{\mathbf{F}}_{\rm BB}}{\arg\min} \left\|\mathbf{F}_{\rm opt} - \mathbf{G}_T\tilde{\mathbf{F}}_{\rm BB}\right\|_{\rm F} \quad \text{s.t.} \quad \left\|\text{diag}\left(\tilde{\mathbf{F}}_{\rm BB}\tilde{\mathbf{F}}_{\rm BB}^H\right)\right\|_0 = \tilde{N}, \quad (42)$$

where $\tilde{\mathbf{F}}_{\rm BB} \in \mathbb{C}^{S \times KU}$ denotes the intermediate BB TP. The constraint in (42) is imposed because the matrix $\tilde{\mathbf{F}}_{\rm BB}$ can have a maximum of $\tilde{N}$ non-zero rows, as there are only $N_{{\rm RF},n}$ RFCs available at each AP, which leads to a block-sparse structure for the matrix $\tilde{\mathbf{F}}_{\rm BB}$. Next, we discuss the framework of designing the hybrid TP by employing the proposed BL-based method corresponding to the problem (42). Initially, the proposed BL-based method of designing the hybrid TP assigns the parameterized Gaussian prior $p\left(\tilde{\mathbf{F}}_{\rm BB}; \boldsymbol{\Delta}\right)$

$$p\left(\tilde{\mathbf{F}}_{\rm BB}; \boldsymbol{\Delta}\right) = \prod_{i=1}^{S} p\left(\tilde{\mathbf{F}}_{\rm BB}(i,:); \delta_i\right) = \prod_{i=1}^{S} \frac{1}{\pi\delta_i} \exp\left(-\frac{\left\|\tilde{\mathbf{F}}_{\rm BB}(i,:)\right\|^2}{\delta_i}\right), \quad (43)$$

to the matrix $\tilde{\mathbf{F}}_{\rm BB}$, where δ_i denotes the hyperparameter associated with the ith row of the matrix $\tilde{\mathbf{F}}_{\rm BB}$, which enforces the row sparsity. The hyperparameter vector $\boldsymbol{\delta}$ is defined as $\boldsymbol{\delta} = [\delta_1, \delta_2, \ldots, \delta_S]^T$ and $\boldsymbol{\Delta} = \text{diag}(\boldsymbol{\delta}) \in \mathbb{R}^{S \times S}$ represents the diagonal matrix of hyper-parameters. Determining $\tilde{\mathbf{F}}_{\rm BB}$ reduces to the estimation of the corresponding hyperparameter vector $\boldsymbol{\delta}$. In principle, one can therefore obtain the maximum likelihood estimate of $\boldsymbol{\delta}$ by maximizing the Bayesian evidence $p(\mathbf{F}_{\rm opt}; \boldsymbol{\delta})$. Nevertheless, the resultant optimization problem is intractable due to its non-convex nature. Consequently, a low-complexity iterative expectation-maximization (EM) algorithm is proposed for the BL-based hybrid TP design. This approach ensures that likelihood maximization is achieved in each iteration and guarantees convergence towards a local optimum. The detailed derivation of the BL-based framework has been relegated to our technical report [46].

Upon reaching the convergence of the EM algorithm, the BL-based RF and BB TPs are obtained as follows. Let $\mathcal{I}$ denote the set of indices for the $\left(\tilde{N}\right)$ hyperparameters having the largest magnitudes. The concatenated optimal BB TP matrix $\mathbf{F}_{\rm BB}^*$ can be extracted from $\tilde{\mathbf{F}}_{\rm BB}$ as $\mathbf{F}_{\rm BB}^* = \tilde{\mathbf{F}}_{\rm BB}(\mathcal{I},:)$. Similarly, one can also obtain the optimal RF TP $\mathbf{F}_{\rm RF}^*$ from the dictionary matrix $\mathbf{G}_T$ as $\mathbf{F}_{\rm RF}^* = \mathbf{G}_T(:,\mathcal{I})$. Following a similar approach, one can derive the digital BB and RF RCs from the FD combiner. The cost function of the BL algorithm has been shown to converge to the optimal solution, which ensures the sparsest representation of the FD TP [47]. Additionally, the EM algorithm provides an advantage for the proposed BL method by ensuring convergence to a fixed point of the log-likelihood function, regardless of the initial state.

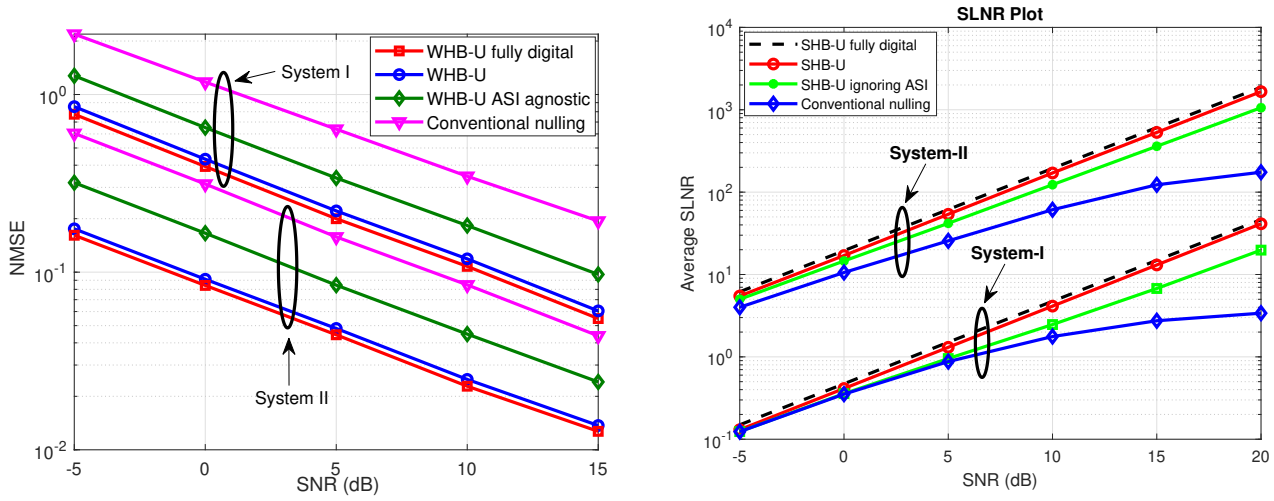

(a) (b)

Fig. 2: Unicast scenario: (a) NMSE comparison of WHB-U and conventional nullification for System-I and System-II; (b) Average SLNR versus SNR for System-I and System-II.

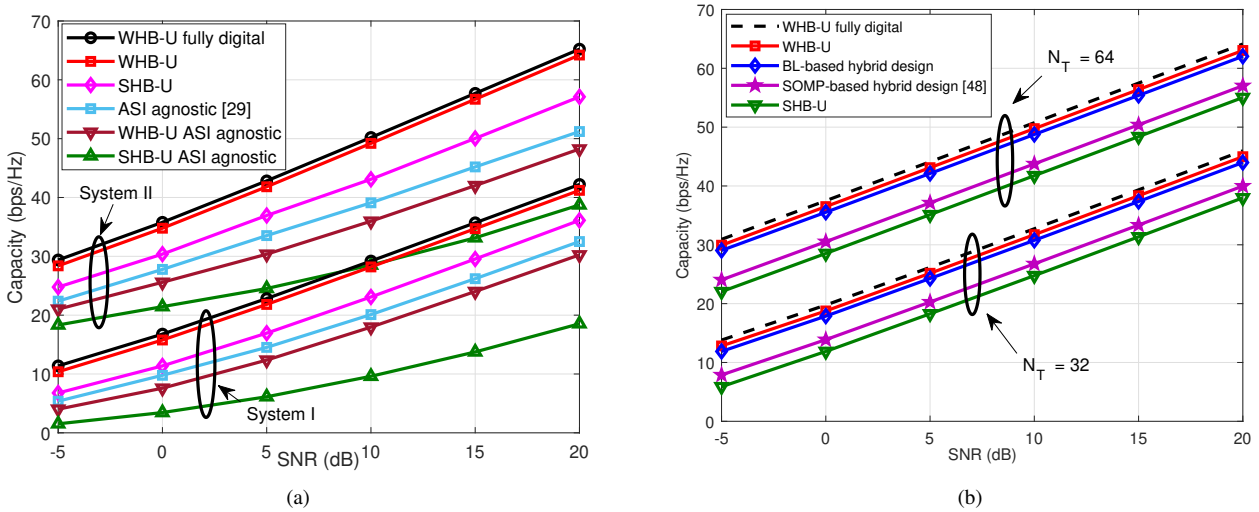

(a) (b)

Fig. 3: Unicast scenario: (a) Capacity comparison of WHB-U and SHB-U schemes for System-I and and System-II; (b) Capacity versus SNR with different number of antennas for System-I.

By contrast, the simultaneous orthogonal matching pursuit (SOMP) [48] based hybrid TP/RC design is sensitive to the choice of the dictionary matrix $\mathbf{G}_T$ as well as to the stopping parameter, which leads to inferior performance. This ensures outstanding performance for the BL algorithm and makes it a compelling technique for designing the hybrid TP/RC in cell-free mmWave MIMO networks.

A. Complexity analysis

The complexity analysis of the proposed cooperative hybrid beamformer design is summarized in this section. Due to a lack of space, the detailed derivations for the computational complexities of the proposed schemes had to be relegated to our technical report [46]. The complexity orders of designing the TP $\mathbf{F}_{\mathrm{BB},u}$ and RC $\mathbf{W}_{\mathrm{BB},u}$ using the WHB scheme are seen to be $\mathcal{O}\left(\left(\tilde{N}\right)^3\right)$ and $\mathcal{O}\left(N_{\mathrm{RF},u}^3\right)$, respectively, which arise due to the matrix inversions in (21) and (24), respectively. Furthermore, one can observe that the complexity order of the SHB scheme is $\mathcal{O}\left(K\left(\tilde{N}\right)^3\right)$. Note that while the computational complexities of the WHB and SHB schemes are similar, the SLNR-based TP design results in a closed-form solution. On the other hand, the complexity order of designing the FD beamformer for both the WHB and SHB schemes are $\mathcal{O}\left(\left(NN_T\right)^3\right)$ and $\mathcal{O}\left(K\left(NN_T\right)^3\right)$,

TABLE II: Simulation parameters of System-I and System-II for cooperative cell-free mmWave MIMO system

Parameter	System-I	System-II
# of APs (N)	2	4
# of users (U)	4	8
# of TAs (N_T)	32	64
# of RAs (N_R)	4	8
# of user groups (G)	2	4
# of users per group (U_g)	2	4
# of RFCs at APs ($N_{\mathrm{RF},n}$)	8	16
# of RFCs at users ($N_{\mathrm{RF},n}$)	2	4
# of streams K	2	2

respectively. Next, using the BL-based framework, the FD TP/RC is decomposed into its constituent RF and BB TPs/RCs, which incurs a complexity order of $\mathcal{O}\left(S^3\right)$ due to the matrix inversion of size $[S \times S]$. However, note that since $S >> NN_T$, the overall complexity of the BL-based hybrid TP/RC can be closely approximated by $\mathcal{O}\left(S^3\right)$. Therefore, one can observe that the WHB and SHB hybrid TP/RC design schemes incur a much-reduced complexity of order $\mathcal{O}\left(\left(\tilde{N}\right)^3\right)$, since we have $\tilde{N} >> NN_T$ in comparison to the BL-based design. However, as mentioned earlier, the BL-based design does not require any knowledge of the individual components of the channel, viz., the AoAs, AoDs, and complex gains of the multipath components.

VI. Simulation results

This section presents our simulation results to illustrate the performance of the cooperative hybrid TP/RC design methods for proposed mitigating the ASI in both unicast and multicast scenarios of cell-free mmWave MIMO networks. In our simulations, we consider a network comprised of $N = 4$ APs and $U = 8$ users that are uniformly distributed in a circular area of radius 300m. The inter-AP distance is 50m. Each of the APs and users has $N_T = 32$ TAs and $N_R = 8$ RAs, respectively. The number of streams K is set to 2 for each user/user group at each AP. These parameters are in line with those of other closely authoritative studies such as [29], [35], [37]. For distances up to 30m, the free-space path-loss exponent of the channels spanning from all the APs to all the users is set to 2. Beyond this distance, the exponent increases to 3.7, as per the standard model [7]. The mmWave MIMO channel $\mathbf{H}_{u,m}$ corresponding to the uth user and nth AP is generated using $L = 6$ multipath components, and the multipath gains $\beta_{u,m}^{l}$ are generated as $\mathcal{CN}(0, 1)$. For our BL-based TP/RC design, the stopping parameters are set to $k_{\max} = 50$ and $\epsilon = 10^{-6}$. We employ practical rectangular pulses with duration $T = 1\mu$s. In all the scenarios considered, we assume that $P_u = P$ for any user u.

A. Unicast hybrid beamforming

We begin with a unicast scenario in the presence of ASI and contrast the NMSE, SLNR and capacity of the various schemes. Fig. 2a plots the average NMSE of the proposed WHB-U scheme for both System I and System II and contrasts its performance under two scenarios: one that is aware of the asynchronous nature of the interference, and another that is agnostic of this effect. One can observe that the proposed hybrid TP/RC design associated with $N_{\mathrm{RF},n} = 8$ and $N_{\mathrm{RF},u} = 2$ RFCs at each AP and user, respectively, performs similarly to the ideal FD design that has $N_{\mathrm{RF},n} = 32$ and $N_{\mathrm{RF},u} = 4$ RFCs. The WHB-U is also seen to lead to a significant NMSE improvement in comparison to its agnostic counterpart that ignores the asynchronous nature of the interference. This demonstrates the degrading effect of ASI on the system's performance and also reflects the fact that the WHB-U scheme is capable of successfully mitigating it. Furthermore, one can also observe that the WHB-U performs better than the conventional nulling scheme [49], which forces the TPs to satisfy the constraint $\tilde{\mathbf{H}}_u \mathbf{F}_{\mathrm{BB},j} = 0, \forall u \neq j$. However, the conventional nulling method fails to completely eliminate the interference in the presence of ASI in (15). Fig. 2b plots the average SLNR versus SNR performance of the SHB-U scheme described in Section III-B for both System-I as well as System-2 and compares it once again to that of the ideal FD, ASI agnostic and conventional nulling counterparts. Once again, the SHB-U performs closer to the ideal FD TP/RC, which echoes the trend observed previously for NMSE minimization. Moreover, observe that the performance of the ASI agnostic SHB-U is close to that of conventional nulling, which indicates the poor performance of the former. This further reiterates the important fact that giving cognizance to the asynchronous nature of interference markedly improves the overall system performance.

B. Capacity analysis of Unicast scenario

Fig. 3a compares the capacities of the WHB-U and SHB-U algorithms both with and without considering the ASI. Note that taking the ASI into account improves the system performance for both designs. Once again, observe that both of the proposed algorithms outperform their respective conventional counterparts. Additionally, we have also compared the proposed TP/RC methods to the hybrid TP of [29] in Fig. 3a. One can observe that the proposed schemes demonstrate a higher capacity than that of [29] as the latter fails to mitigate the degrading effects of ASI.

Fig. 3b compares the capacity of the BL-based TP/RC design both to that of the WHB-U and SHB-U based hybrid TP/RC as well as to the SOMP algorithm based hybrid TP and ideal FD beamformer for $N_T = 32$ and $N_T = 64$ TAs at each AP. Notably, the BL-based approach achieves a performance similar to the FD TP/RC design. However, while the former only requires $N_{\mathrm{RF},n} = 8$ RFCs, the latter has $N_{\mathrm{RF},n} = 32$ and $N_{\mathrm{RF},n} = 64$ RFCs for $N_T = 32$ and $N_T = 64$ TAs, respectively. This clearly shows the advantage of the former in practical implementations. Furthermore, the BL-based TP/RC design provides a significant spectral efficiency gain in comparison to the SOMP-based design. This arises due to the fact that the BL

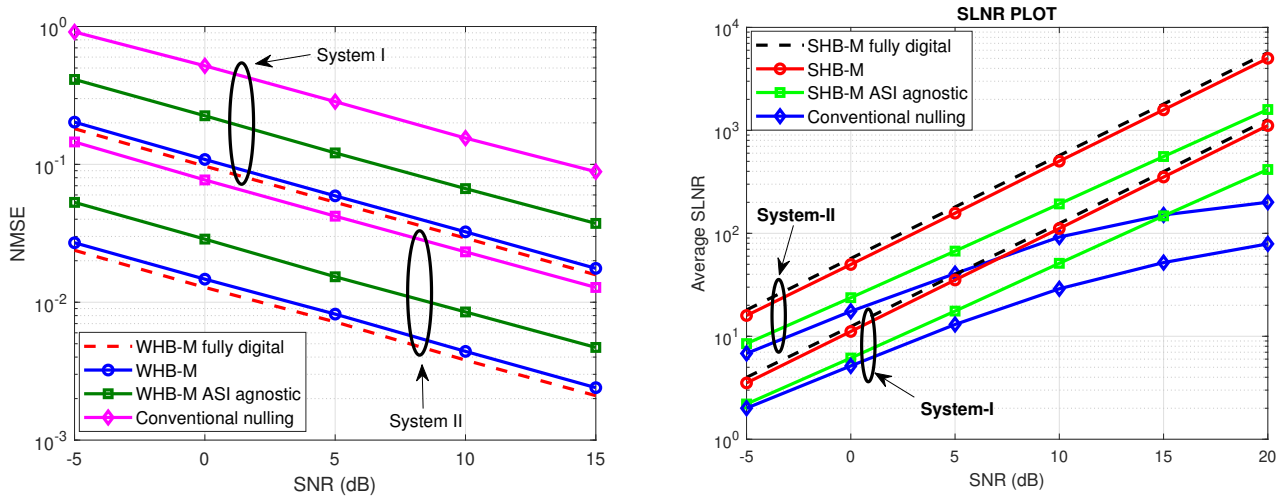

(a) (b)

Fig. 4: Multicast scenario: (a) NMSE versus SNR for System-I and System-II; (b) Average SLNR versus SNR for System-I and System-II.

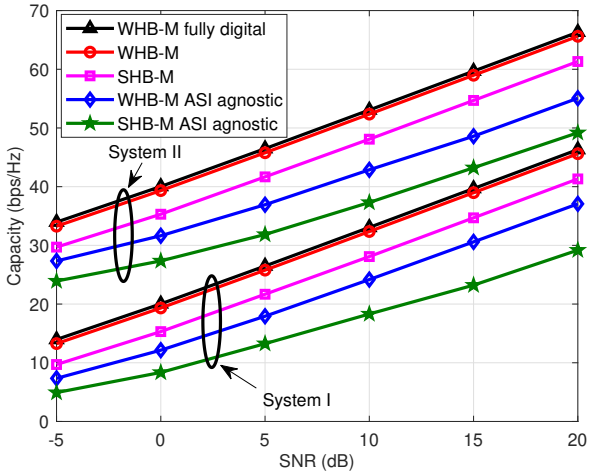

Fig. 5: Capacity versus SNR for System-I and System-II.

algorithm has improved sparse signal recovery properties in comparison to the SOMP. Furthermore, the performance of the latter scheme is highly sensitive to the choice of both the dictionary matrix and to the stopping criterion. This interesting outcome can be attributed to the low-rank nature of the mmWave MIMO channel, arising due to the fact that it only has a few multipath components, which is exploited by the BL algorithm. As a result, an approximation to the ideal FD beamformer can be achieved by combining only a few beams corresponding to the transmit/receive array manifold vectors. Note that the BL-based framework eliminates the need for complete knowledge of AoDs/AoAs along with their corresponding path gains for the BB and RF TP/RC design. Additionally, the results also highlight the advantages of large-scale antenna arrays in the mmWave frequency range. It is evident that the performance of the WHB-U and SHB-U schemes improves significantly for an increased number of TAs at the APs.

C. Beamforming for multicast scenarios

Fig. 4a compares the NMSE performance of the WHB-M scheme for $G = 2$ user groups and $U_g = 2$ users in each group. Once again, observe that the WHB-M scheme is capable of mitigating the ASI and achieve a performance closer to the ideal FD design. Furthermore, the proposed WHB-M scheme outperforms conventional nulling, because it accounts for the asynchronous nature of interference. Fig. 4b plots the SLNR performance of the proposed SHB-M TP/RC design for both System-I and System-II in the multicast system. Once again, the SHB-M performs closer to the ideal FD TP/RC, which echoes the trend observed previously for the unicast scenario. Fig. 5 compares the capacity of the proposed WHB-M and SHB-M techniques to that of the FD design and conventional algorithms. Furthermore, one can observe that the proposed TP/RC schemes are capable of mitigating the ASI.

VII. CONCLUSION

Cooperative hybrid TPs and RCs were designed for cell-free mmWave MIMO networks for mitigating the effect of ASI, while considering both unicast as well as multicast scenarios. Initially, the WHB-U and SHB-U TP/RC design techniques were proposed for a unicast scenario, which efficiently mitigated the ASI. Subsequently, the proposed techniques were extended to a multicast scenario, wherein all the users of a multicast group seek the same information. Next, a BL-based hybrid TP/RC design was conceived that eliminates the need for complete knowledge of the AoDs/AoAs of the mmWave MIMO channel, along with

their path gains. Our simulation results exhibited enhanced NMSE as well as spectral efficiency for the proposed WHB and SHB techniques. The schemes advocated were also seen to significantly outperform conventional nulling that ignores the asynchronous nature of interference. The proposed hybrid TP/RC designs have a reduced complexity and are capable of simultaneously supporting a higher number of users than the ZF-based methods. This renders them eminently suitable for the practical implementation of cell-free mmWave MIMO networks.

REFERENCES

[1] R. W. Heath, N. Gonzalez-Prelcic, S. Rangan, W. Roh, and A. M. Sayeed, "An overview of signal processing techniques for millimeter wave MIMO systems," *IEEE Journal of Selected Topics in Signal Processing*, vol. 10, no. 3, pp. 436–453, 2016.

[2] H. Shokri-Ghadikolaei, C. Fischione, G. Fodor, P. Popovski, and M. Zorzi, "Millimeter wave cellular networks: A MAC layer perspective," *IEEE Transactions on Communications*, vol. 63, no. 10, pp. 3437–3458, 2015.

[3] I. A. Hemadeh, K. Satyanarayana, M. El-Hajjar, and L. Hanzo, "Millimeter-wave communications: Physical channel models, design considerations, antenna constructions, and link-budget," *IEEE Communications Surveys & Tutorials*, vol. 20, no. 2, pp. 870–913, 2017.

[4] B. P. Sahoo, C.-C. Chou, C.-W. Weng, and H.-Y. Wei, "Enabling millimeter-wave 5G networks for massive IoT applications: A closer look at the issues impacting millimeter-waves in consumer devices under the 5G framework," *IEEE Consumer Electronics Magazine*, vol. 8, no. 1, pp. 49–54, 2018.

[5] T. Bai and R. W. Heath, "Coverage and rate analysis for millimeter-wave cellular networks," *IEEE Transactions on Wireless Communications*, vol. 14, no. 2, pp. 1100–1114, 2014.

[6] A. Mesodiakaki, F. Adelantado, L. Alonso, M. Di Renzo, and C. Verikoukis, "Energy-and spectrum-efficient user association in millimeter-wave backhaul small-cell networks," *IEEE Transactions on Vehicular Technology*, vol. 66, no. 2, pp. 1810–1821, 2016.

[7] H. Q. Ngo, A. Ashikhmin, H. Yang, E. G. Larsson, and T. L. Marzetta, "Cell-free massive MIMO versus small cells," *IEEE Transactions on Wireless Communications*, vol. 16, no. 3, pp. 1834–1850, 2017.

[8] J. Zhang, S. Chen, Y. Lin, J. Zheng, B. Ai, and L. Hanzo, "Cell-free massive MIMO: A new next-generation paradigm," *IEEE Access*, vol. 7, pp. 99 878–99 888, 2019.

[9] S. Elhoushy, M. Ibrahim, and W. Hamouda, "Cell-free massive MIMO: A survey," *IEEE Communications Surveys & Tutorials*, vol. 24, no. 1, pp. 492–523, 2021.

[10] Ö. T. Demir, E. Björnson, L. Sanguinetti *et al.*, "Foundations of user-centric cell-free massive MIMO," *Foundations and Trends® in Signal Processing*, vol. 14, no. 3-4, pp. 162–472, 2021.

[11] E. Björnson and L. Sanguinetti, "Making cell-free massive MIMO competitive with MMSE processing and centralized implementation," *IEEE Transactions on Wireless Communications*, vol. 19, no. 1, pp. 77–90, 2019.

[12] S. Rangan, T. S. Rappaport, and E. Erkip, "Millimeter-wave cellular wireless networks: Potentials and challenges," *Proceedings of the IEEE*, vol. 102, no. 3, pp. 366–385, 2014.

[13] L. Wei, R. Q. Hu, Y. Qian, and G. Wu, "Key elements to enable millimeter wave communications for 5G wireless systems," *IEEE Wireless Communications*, vol. 21, no. 6, pp. 136–143, 2014.

[14] S. Kutty and D. Sen, "Beamforming for millimeter wave communications: An inclusive survey," *IEEE Communications Surveys & Tutorials*, vol. 18, no. 2, pp. 949–973, 2015.

[15] O. El Ayach, S. Rajagopal, S. Abu-Surra, Z. Pi, and R. W. Heath, "Spatially sparse precoding in millimeter wave MIMO systems," *IEEE Transactions on Wireless Communications*, vol. 13, no. 3, pp. 1499–1513, 2014.

[16] P. Zheng, X. Xie, and G. Qu, "Suppressed inter-cell asynchronous interference by delay-tolerance SLNR precoding," in *2010 The 12th International Conference on Advanced Communication Technology (ICACT)*, vol. 1. IEEE, 2010, pp. 627–632.

[17] M. H. Hassan, M. J. Hossain, and V. K. Bhargava, "Cooperative beamforming for cognitive-radio-based broadcasting systems in presence of asynchronous interference," *IEEE Transactions on Vehicular Technology*, vol. 66, no. 3, pp. 2311–2323, 2016.

[18] X. Cai, Z. Huang, and B. Li, "Asynchronous and non-stationary interference cancellation in multiuser interference channels," *IEEE Transactions on Wireless Communications*, vol. 20, no. 8, pp. 4976–4989, 2021.

[19] A. Michaloliakos, W.-C. Ao, and K. Psounis, "Joint user-beam selection for hybrid beamforming in asynchronously coordinated multi-cell networks," in *2016 Information Theory and Applications Workshop (ITA)*. IEEE, 2016, pp. 1–10.

[20] R. Zhang and L. Hanzo, "Cooperative downlink multicell preprocessing relying on reduced-rate back-haul data exchange," *IEEE Transactions on Vehicular Technology*, vol. 60, no. 2, pp. 539–545, 2010.

[21] Z. Xiang, M. Tao, and X. Wang, "Coordinated multicast beamforming in multicell networks," *IEEE Transactions on Wireless Communications*, vol. 12, no. 1, pp. 12–21, 2012.

[22] S. He, Y. Huang, L. Yang, and B. Ottersten, "Coordinated multicell multiuser precoding for maximizing weighted sum energy efficiency," *IEEE Transactions on Signal Processing*, vol. 62, no. 3, pp. 741–751, 2014.

[23] E. Nayebi, A. Ashikhmin, T. L. Marzetta, H. Yang, and B. D. Rao, "Precoding and power optimization in cell-free massive MIMO systems," *IEEE Transactions on Wireless Communications*, vol. 16, no. 7, pp. 4445–4459, 2017.

[24] M. Attarifar, A. Abbasfar, and A. Lozano, "Modified conjugate beamforming for cell-free massive MIMO," *IEEE Wireless Communications Letters*, vol. 8, no. 2, pp. 616–619, 2019.

[25] E. Björnson and L. Sanguinetti, "Scalable cell-free massive MIMO systems," *IEEE Transactions on Communications*, vol. 68, no. 7, pp. 4247–4261, 2020.

[26] Y. Cao, P. Wang, K. Zheng, X. Liang, D. Liu, M. Lou, J. Jin, Q. Wang, D. Wang, Y. Huang *et al.*, "Experimental performance evaluation of cell-free massive MIMO systems using COTS RRU with OTA reciprocity calibration and phase synchronization," *IEEE Journal on Selected Areas in Communications*, 2023.

[27] Q. Hou, S. He, Y. Huang, H. Wang, and L. Yang, "Joint user scheduling and hybrid precoding design for MIMO C-RAN," in *2017 9th International Conference on Wireless Communications and Signal Processing (WCSP)*. IEEE, 2017, pp. 1–6.

[28] J. Kim, S.-H. Park, O. Simeone, I. Lee, and S. S. Shitz, "Joint design of fronthauling and hybrid beamforming for downlink C-RAN systems," *IEEE Transactions on Communications*, vol. 67, no. 6, pp. 4423–4434, 2019.

[29] C. Feng, W. Shen, J. An, and L. Hanzo, "Weighted sum rate maximization of the mmWave cell-free MIMO downlink relying on hybrid precoding," *IEEE Transactions on Wireless Communications*, vol. 21, no. 4, pp. 2547–2560, 2021.

[30] Z. Wang, M. Li, R. Liu, and Q. Liu, "Joint user association and hybrid beamforming designs for cell-free mmWave MIMO communications," *IEEE Transactions on Communications*, vol. 70, no. 11, pp. 7307–7321, 2022.

[31] Y. He, M. Shen, R. Wang, and X. Liu, "Energy efficient hybrid precoder for cell-free wideband mmWave massive MIMO systems," *IEEE Communications Letters*, 2023.

[32] X. Ma, D. Zhang, M. Xiao, C. Huang, and Z. Chen, "Cooperative beamforming for RIS-aided cell-free massive MIMO networks," *IEEE Transactions on Wireless Communications*, 2023.

[33] G. Femenias and F. Riera-Palou, "Cell-free millimeter-wave massive MIMO systems with limited fronthaul capacity," *IEEE Access*, vol. 7, pp. 44 596–44 612, 2019.

[34] M. Jafri, S. Srivastava, N. K. D. Venkategowda, A. K. Jagannatham, and L. Hanzo, "Cooperative hybrid transmit beamforming in cell-free mmWave MIMO networks," *IEEE Transactions on Vehicular Technology*, vol. 72, no. 5, pp. 6023–6038, 2023.

[35] J. Li, M. Liu, P. Zhu, D. Wang, and X. You, "Impacts of asynchronous reception on cell-free distributed massive MIMO systems," *IEEE Transactions on Vehicular Technology*, vol. 70, no. 10, pp. 11 106–11 110, 2021.

[36] G. Li, S. Wu, C. You, W. Zhang, G. Shang, and X. Zhou, "Cell-free massive MIMO-OFDM: Asynchronous reception and performance analysis," *IEEE Internet of Things Journal*, 2023.

[37] J. Zheng, J. Zhang, J. Cheng, V. C. Leung, D. W. K. Ng, and B. Ai, "Asynchronous cell-free massive MIMO with rate-splitting," *IEEE Journal on Selected Areas in Communications*, vol. 41, no. 5, pp. 1366–1382, 2023.

[38] J.-C. Guo, Q.-Y. Yu, W.-B. Sun, and W.-X. Meng, "Robust efficient hybrid pre-coding scheme for mmwave cell-free and user-centric massive MIMO communications," *IEEE Transactions on Wireless Communications*, vol. 20, no. 12, pp. 8006–8022, 2021.

[39] J. Kassam, D. Castanheira, A. Silva, R. Dinis, and A. Gameiro, "Distributed hybrid equalization for cooperative millimeter-wave cell-free massive MIMO," *IEEE Transactions on Communications*, vol. 70, no. 8, pp. 5300–5316, 2022.

[40] Z. Cheng, Z. Wei, H. Li, and H. Yang, "SLNR-based beamspace precoding and beam selection for wideband mmwave massive MIMO," *IEEE Communications Letters*, vol. 26, no. 2, pp. 478–482, 2021.

[41] L. Pang, W. Wu, Y. Zhang, Y. Yuan, Y. Chen, A. Wang, and J. Li, "Joint power allocation and hybrid beamforming for downlink mmWave-NOMA systems," *IEEE Transactions on Vehicular Technology*, vol. 70, no. 10, pp. 10 173–10 184, 2021.

[42] S. Tharranetharan and J. Hossain, "Data rate fairness cooperative beamforming techniques for cognitive radio systems in the presence of asynchronous interferences," *IEEE Transactions on Communications*, vol. 64, no. 10, pp. 4083–4096, 2016.

[43] L. Du, L. Li, H. Q. Ngo, T. C. Mai, and M. Matthaiou, "Cell-free massive MIMO: Joint maximum-ratio and zero-forcing precoder with power control," *IEEE Transactions on Communications*, vol. 69, no. 6, pp. 3741–3756, 2021.

[44] S. P. Boyd and L. Vandenberghe, *Convex optimization*. Cambridge university press, 2004.

[45] A. Tarighat, M. Sadek, and A. H. Sayed, "A multi user beamforming scheme for downlink MIMO channels based on maximizing signal-to-leakage ratios," in *Proceedings.(ICASSP'05). IEEE International Conference on Acoustics, Speech, and Signal Processing, 2005.*, vol. 3. IEEE, 2005, pp. iii–1129.

[46] M. Jafri, S. Srivastava, P. Kumar, A. K. Jagannatham, and L. Hanzo, "Technical report: Cooperative hybrid beamforming for the mitigation of realistic asynchronous interference in cell-free mmWave MIMO networks," *IIT Kanpur, Tech. Rep.*, 2023 [Online]. [Online]. Available: https://www.iitk.ac.in/mwn/documents/MWNLAB_TR_CellFreeASI.pdf

[47] D. P. Wipf and B. D. Rao, "Sparse Bayesian learning for basis selection," *IEEE Transactions on Signal processing*, vol. 52, no. 8, pp. 2153–2164, 2004.

[48] A. Alkhateeb, G. Leus, and R. W. Heath, "Limited feedback hybrid precoding for multi-user millimeter wave systems," *IEEE Transactions on Wireless Communications*, vol. 14, no. 11, pp. 6481–6494, 2015.

[49] G. Foschini, "The value of coherent base station coordination," in *Conference on Information Sciences and Systems (CISS), Johns Hopkins University, Mar. 2005*, 2005.

MEESAM JAFRI (Student Member, IEEE) received the B.E. degree in electronics and communication engineering from Jamia Millia Islamia, New Delhi, India, in 2016, and the M.Tech. degree in communication and information technology from the National Institute of Technology Srinagar, India, in 2018. He is currently pursuing the Ph.D. degree with the Department of Electrical Engineering, Indian Institute of Technology Kanpur, Kanpur, India. His research interests include coordinated beamforming in 5G wireless systems, mmWave communication, orthogonal time-frequency space (OTFS), radar signal processing, and joint radar and communication (RadCom). He was awarded Qualcomm Innovation Fellowship (QIF) from Qualcomm, in 2022.

SURAJ SRIVASTAVA (Member, IEEE) received the M.Tech. degree in Electronics and Communication Engineering from Indian Institute of Technology Roorkee, India, in 2012, and Ph.D. degree in Electrical Engineering from Indian Institute of Technology Kanpur, Kanpur, India, in 2022. From July 2012 to November 2013, he was employed as a Staff-I systems design engineer with Broadcom Research India Pvt. Ltd., Bangalore, and from November 2013 to December 2015, he was employed as a lead engineer with Samsung Research India, Bangalore where he worked on developing layer-2 of the 3G UMTS/WCDMA/HSDPA modem. His research interests include applications of Sparse Signal Processing in 5G Wireless Systems, mmWave and Tera-Hertz Communication, Orthogonal Time-Frequency Space (OTFS), Joint Radar and Communication (RadCom), Optimization and Machine Learning. He was awarded Qualcomm Innovation Fellowship (QIF) in year 2018 and 2022 from Qualcomm. He was also awarded Outstanding Ph.D. Thesis and Outstanding Teaching Assistant awards from IIT Kanpur.

PANKAJ KUMAR received the B.E. degree in electronics and communication engineering from the Army Institute of Technology, Pune, India, and the M.Tech. degree in electrical engineering with specialization in signal processing, communication, and networking from the Indian Institute of Technology Kanpur, India. He is currently pursuing a Ph.D. in wireless communications from the University of Southampton, UK. His research interests include mmWave communications, Hybrid beamforming, cell-free networks, and Integrated Sensing and Communication (ISAC).

ADITYA K. JAGANNATHAM (Senior Member, IEEE) received the bachelor's degree from the Indian Institute of Technology, Bombay, and the M.S. and Ph.D. degrees from the University of California at San Diego, San Diego, CA, USA. From April 2007 to May 2009, he was employed as a Senior Wireless Systems Engineer with Qualcomm Inc., San Diego, where he was a part of the Qualcomm CDMA Technologies Division. He is currently a Professor with the Department of Electrical Engineering, IIT Kanpur, where he also holds the Arun Kumar Chair Professorship. His research interests include next generation wireless cellular and WiFi networks, with a special emphasis on various 5G technologies, such as massive MIMO, mmWave MIMO, FBMC, NOMA, as well as emerging 6G technologies, such as OTFS, IRS, THz systems, and VLC. He has been twice awarded the P. K. Kelkar Young Faculty Research Fellowship for excellence in research, received multiple Qualcomm Innovation Fellowships in 2018 and 2022, the IIT Kanpur Excellence in Teaching Award, the CAL(IT)2 Fellowship at the University of California at San Diego, the Upendra Patel Achievement Award at Qualcomm San Diegom and the Qualcomm 6G UR India Gift.

LAJOS HANZO (FIEEE'04) received Honorary Doctorates from the Technical University of Budapest (2009) and Edinburgh University (2015). He is a Foreign Member of the Hungarian Science-Academy, Fellow of the Royal Academy of Engineering (FREng), of the IET, of EURASIP and holds the IEEE Eric Sumner Technical Field Award. For further details please see http://www-mobile.ecs.soton.ac.uk/, https://en.wikipedia.org/wiki/Lajos_Hanzo.